M M-2798(cp)
CONF-801074--2

# AN OVERVIEW OF SURFACE STUDIES O

# HIGH ENERGY MATERIALS AT MOUND

W. E. Moddeman, L. W. Collins, P. S. Wang and L. D. Haws

Monsanto Research Corporation
Mound Facility*
Miamisburg, Ohio 45342

and

T. N. Wittberg
University of Dayton Research Institute
Dayton, Ohio 45469



*Mound Facility is operated by Monsanto Research Corporation for the U. S. Department of Energy under Contract No. DE-AC04-76-DP00053.

## DISCLAIMER

ABSTRACT

Since 1975 Mound has been examining the surface structure of high energy materials and the interaction of these materials with various metal containers. The high energy materials that have been studied include: the pyrotechnic $TiH_x/KClO_4$, the $Al/Cu_2O$ machinable thermite, the PETN, HMX and RDX explosives, and two plastic bonded explosives (PBX). Aluminum and alloys of Fe, Ni and Cr have been used as the containment materials. Two aims in this research are: (1) the elucidation of the mechanism of pyrotechnic ignition and (2) the compatibility of high energy materials with their surroundings. Exciting and new information has been generated by coupling Auger electron spectroscopy (AES) and x-ray photoelectron spectroscopy (XPS) with thermal data. In particular, AES and XPS studies on the pyrotechnic materials and on thermites have shown the mechanism of ignition to be nearly independent of the type of oxidizer present but directly related to surface chemistry of the fuels. In studies on the two PBX's, PBX-9407 and LX-16, it was concluded that the Exon coating on 9407 was complete and $\geq$100Å; whereas in LX-16, the coating was <100Å or even incomplete. AES and scanning Auger have been used to characterize the surface composition and oxide thickness for an iron-nickel alloy and showed the thicker oxides to have the least propensity for atmospheric hydrocarbon adsorption. Data will be presented and illustrations made which highlight this new approach to studying ignition and compatibility of high energy materials. Finally, the salient features of the X-SAM-800 purchased by Mound will be discussed in light of future studies on high energy materials.

## I. INTRODUCTION

Mound has been examining the surface structure of high energy (HE) materials for the past five years. The main emphasis has been on pyrotechnics and explosives (or composite explosives). The HE materials that have been studied include the pyrotechnic fuels [1-9]: $TiH_x$ ($0.15 \leq x \leq 1.95$), Al, Fe, and B; the pyrotechnic oxidizers [10,11]: $KClO_4$, $Cu_2O$, and $K_2CrO_4$; the pyro blends [7-9]: $TiH_x/KClO_4$, $Fe/KClO_4$ and $Al/Cu_2O$; the explosives [12]: PETN, HMX and RDX; and the PBX's: 9407 and LX-16 [12]. Various surface analysis techniques, such as XPS, (x-ray photoelectron spectroscopy), AES (Auger electron spectroscopy) and ISS (ion scattering spectroscopy) have been applied to characterize the surface of these energetic materials with surprising success. In this paper we survey the results obtained thus far and take the opportunity to outline future studies. The results to be discussed are divided into pyrotechnic, explosive and compatibility studies. Details of the surface analysis equipment and sample preparation can be found in each of the quoted references.

## II. RESULTS AND DISCUSSION:

### A. Pyrotechnic Mixtures

Pyrotechnics are mechanical mixtures of a metal fuel and an unstable oxidizer. The pyrotechnic reaction produces primarily condensible products plus heat, light, and/or sound. Of course, the exothermic energy from the reactions is used to do work. The work on the Ti and Al fuels, the $KClO_4$ oxidizers, and the $Al/Cu_2O$ thermite is discussed below in some detail.

1. Ti Fuel

Unprotected titanium metal powder is pyrophoric; that is, a fresh metal surface of titanium will ignite spontaneously in air at room temperature. However, if the metal powder is passivated, e.g., with its native oxide, oxidation rates become negligible so that the powder is stabilized to temperatures in excess of 500°C.

DTA curves [8] for titanium powder ($TiH_{0.15}$) and for the $TiH_{0.15}$ mixed with $KClO_4$, $KIO_4$, $KClO_3$, or $RbClO_4$ oxidizers have shown the exothermic oxidation reactions for these pyrotechnic systems were relatively slow until the temperature exceeded 500° when the reactions became self-sustaining, i.e., ignition occurred. These data establish that thermal ignition of titanium based pyrotechnics is controlled by processes associated with the fuel and is relatively independent of the oxidizer.

AES surface scans have been recorded [8] for a passivated titanium foil sample as a function of temperature and the ratio of the intensity of titanium to oxygen was measured. This ratio is shown again [8] as a function of temperature in Figure 1. The increase in the Ti/O ratio beginning just below 300°C is characteristic of the dissolution of the oxides of titanium into the metal substrate. This is indicative of an increase in surface reactivity due to increased availability of unoxidized titanium metal.

While AES clearly indicates the dissolution process, it does not provide any direct evidence for changes in the oxidation state of

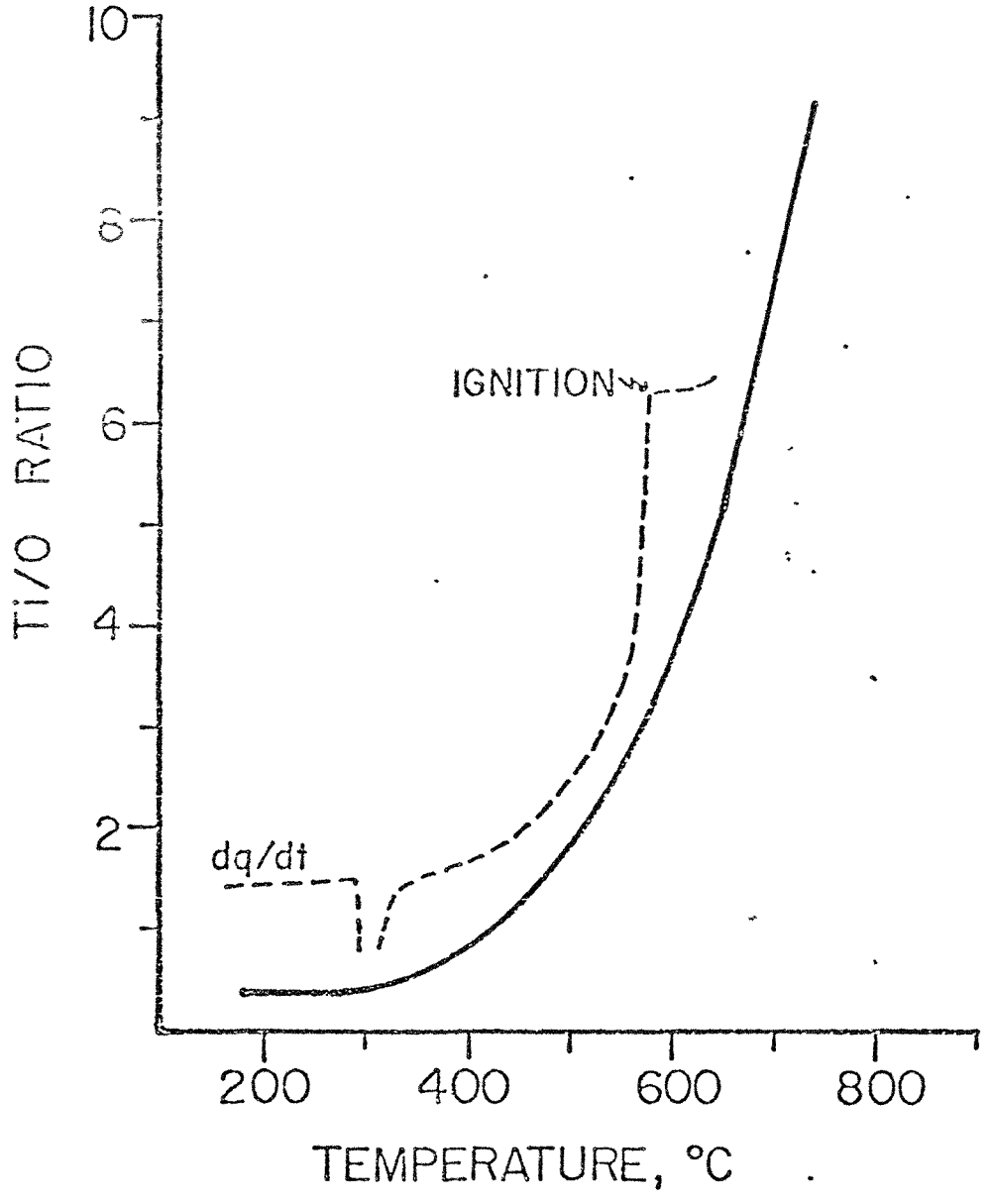


Figure 1 - Ratio of Ti L-MM Auger (418 eV) line to O K-LL (510 eV) line as a function of temperature.

titanium. The O 1s and Ti 2p spectra were recorded at different temperatures in order to study changes in the surface chemistry during dissolution [7]. These data are plotted in Figure 2 and show: (1) that the $Ti^{\circ}/O^{-2}$ ratio begins to increase at 350° which is in good agreement with the AES data; (2) that the $Ti^{+4}/O^{-2}$ ratio begins to decline at ~300°C coincident with the increase in $Ti^{\circ}/O^{-2}$ and $Ti^{+n}/O^{-2}$ ratios; and (3) interestingly, that the $Ti^{+n}/O^{-2}$ ratio does not peak until a temperature of 450° is attained. Thus, we conclude from this XPS data that the dissolution process proceeds through the formation of lower titanium oxides.

It should be noted that ultra high vacuums were used in generating the AES ans XPS data. In normal oxidizing environments, such as those used in generating the thermoanalytical data and in pyrotechnic blends, the replacement of the native oxide is sufficiently rapid between 300° and 500° to keep the active titanium surface concentration very low. This reoxidation of the surface is indicated by DSC as a weak exotherm which we have superimposed on the Auger data in Figure 2.

These data then provide a basis for understanding the chemical processes associated with the thermal ignition of titanium based pyrotechnics [8]. The rapid oxidation reaction necessary to generate sufficient heat for self-sustained reaction is controlled by the availability of reactive titanium at the surface of the fuel particles. At temperatures below 500°, the dissolution reaction of the surface oxide is relatively slow so that there is insufficient fuel available for sustained oxidation in the DTA sample configura-

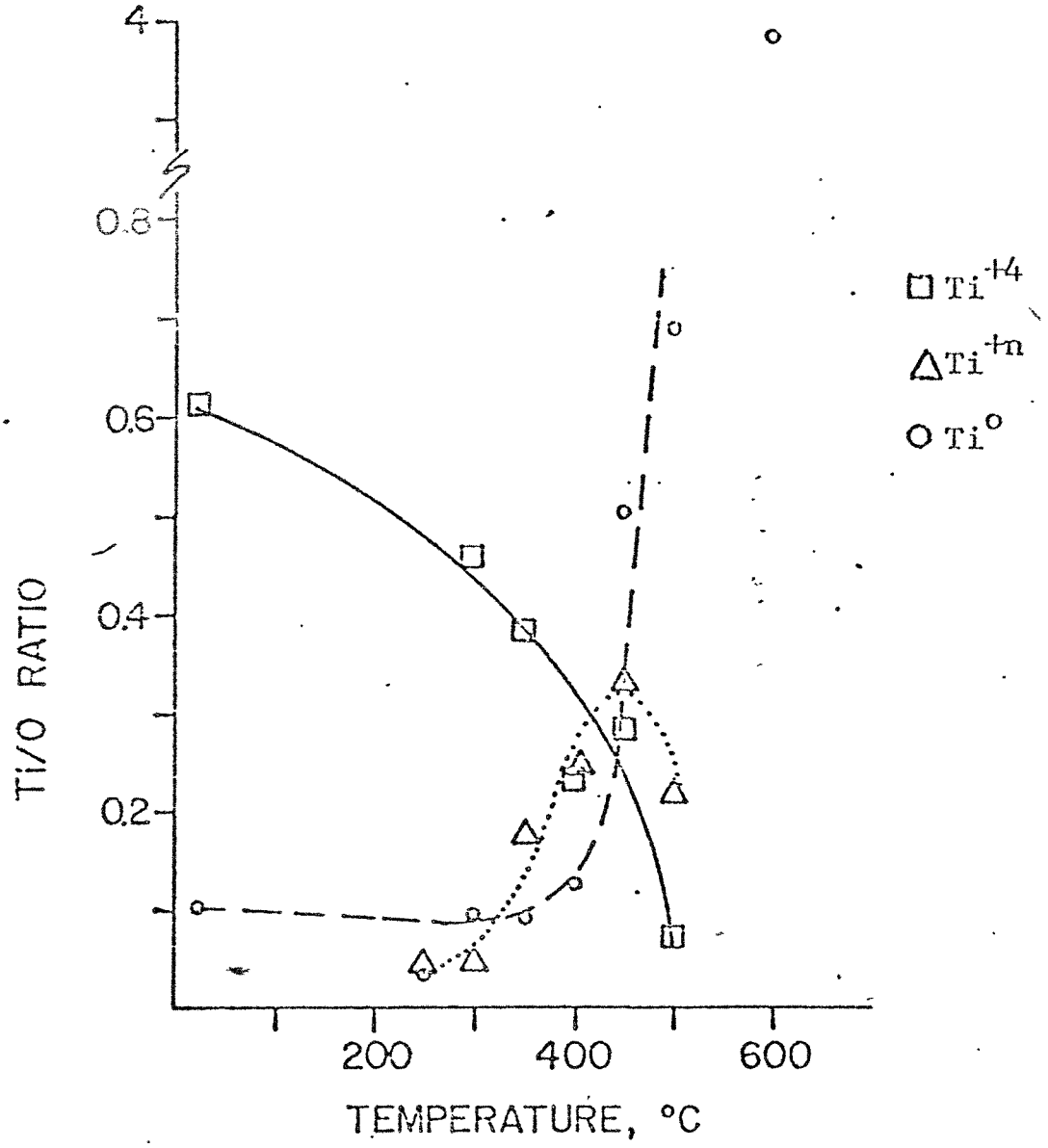


Figure 2 - Ratio of the Ti $2p_{3/2}$ line to the O 1s line for $O^{-2}$ as a function of temperature.

tion. At temperatures in excess of 500°, the dissolution becomes rapid enough to expose sufficient reactive titanium on the surface to sustain ignition. Thus, the ignition process is almost seemingly kinetically controlled by the dissolution of the titanium oxides with the concomitant production of reactive titanium on the surface [8].

2. Aluminum

Aluminum, like titanium, has an oxide coating which stabilizes the very reactive metal against further oxidation until relatively high temperatures are reached. The oxidation process is again controlled by the availability of reactive metal on the surface. When the unoxidized aluminum is exposed to even trace quantities of oxygen, it rapidly reacts. This has been shown by the previously taken TGA data [8]. A gain in mass begins at about 600° and, holding at that temperature, we can observe an increase in oxide thickness to a maximum of ∿4000Å. The oxide coating has also been shown to remain intact through heating cycles to temperatures of 1000°C; the powder remains unchanged in appearance after heating, whereas other metal powders, such as the titanium, flow together upon melting.

The oxidation process occurring at about 600°, which is indicated by the thermoanalytical techniques, corresponds to an increase in the concentration of unreacted aluminum at the surface of the particles. This increase in concentration is shown directly by the increase in the Al/O ratio versus temperature plot presented in Figure 3 which was obtained by AES [8]. Since the oxide coating remains intact, this increase must be due to diffusion of the metal to the surface rather than an oxide dissolution process as observed

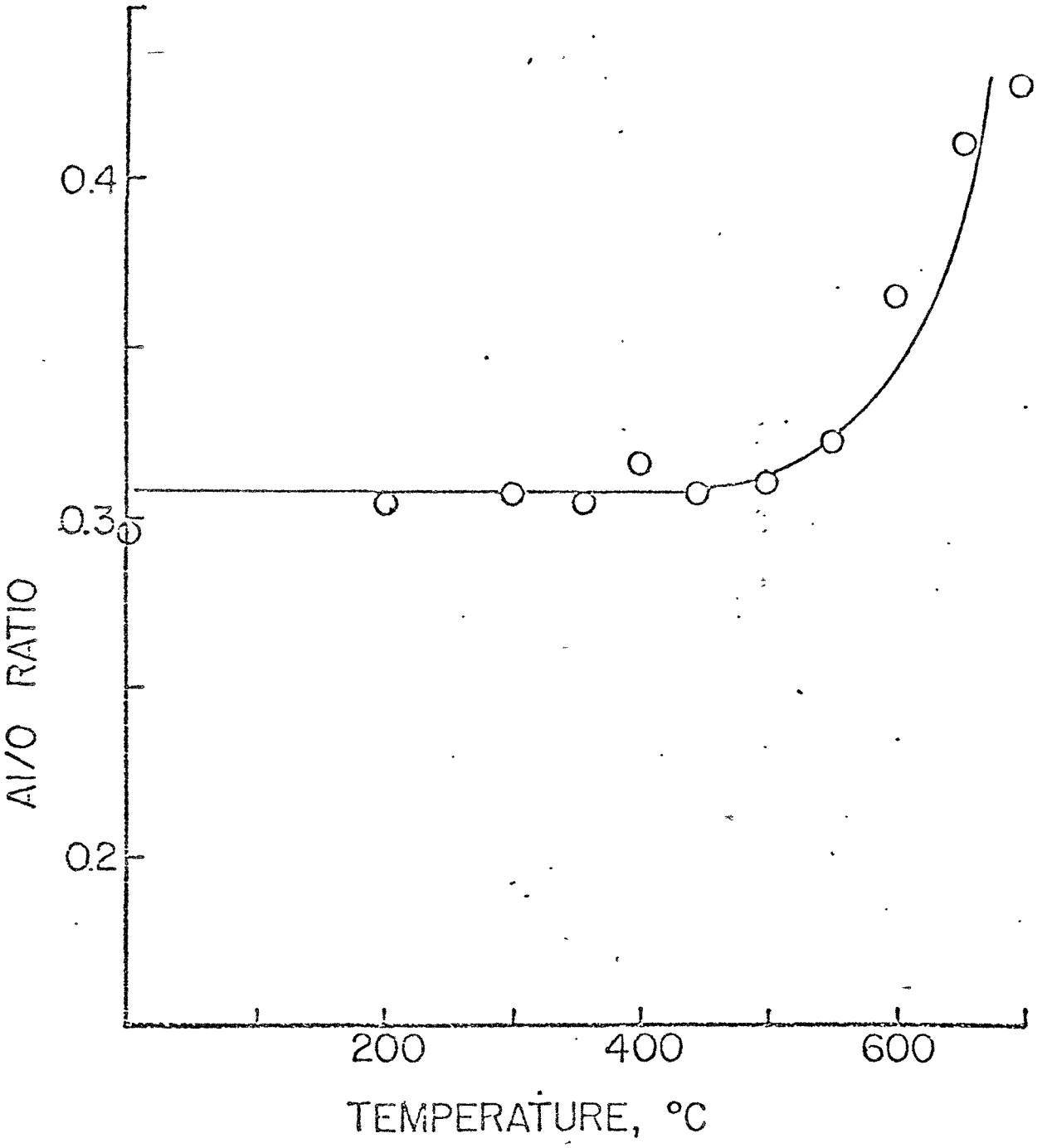


Figure 3 - Ratio of the Al K-LL Auger line (1396 eV) to the O K-LL line (509 eV) as a function of temperature.

for the titanium. The continued increase in oxide thickness opposes the increase in the diffusion rate as the temperature increases. Therefore, this type of process is less likely to kinetically control thermal ignition in aluminum based pyrotechnics than a dissolution process, such as in a titanium based one.

When aluminum was mixed with $Cu_2O$ to form a consolidated pellet, DTA analysis showed [8] that ignition occurred at 545°C. A strong endotherm just prior to ignition of the consolidated pellet (not present in powdered blend [8]) is an indication of a change in the material due to hot pressing used to form the consolidated pellet. The nature of this endotherm is indicative of Al-Cu alloy melting. Thus, the presence of the endotherm in the DTA curve for consolidated thermite indicates that the Al-Cu alloy was formed during the consolidation process.

Ignition of the consolidated thermite seems to depend on the generation of free aluminum at the particle surface. This aluminum can then alloy with copper from the $Cu_2O$. Ignition can occur due to heat generated by the oxidation of the alloy rather than aluminum. The phase change at 540° apparently makes the alloy oxidation reaction favorable; it can generate the heat to achieve ignition of the thermite reaction which is thought to occur at higher temperatures.

### 3. $KClO_4$ Oxidizer

The characterization of the surface chemistry of perchlorate oxidizers has been shown to be difficult to obtain [1,13]. Upon irradiation with the electrons [1] or x-rays [1,13] the $ClO_4^-$ species has been

shown to decompose. AES analysis of $KClO_4$ excited with electrons of current densities of <0.1 $mA/mm^2$ shows rapid and almost complete degradation to KCl. Figure 4 illustrates the Cl 2p XPS spectra of $KClO_4$ taken as a function of x-irradiation time [10,22]. This study was done at room temperature. The sample was prepared by pressing $KClO_4$ with finger pressure onto a thin In foil. In the figure, at time of irradiation equal to ∿1 min, the main photopeak at 209 eV binding energy is due to the photoelectrons ejected by the interaction of the primary photons of the Mg ($MgK_{1,2}$) with the chlorine 2p electrons of $KClO_4$. The photopeak centered at ∿201 eV is due to the chlorine 2p photoelectrons of $KClO_4$ excited at $MgK_{\alpha 3,4}$ satellite photons from the anode. This satellite contribution is less than 10 percent of the photopeak at 209 eV. For time equal to ∿1 min, the residual $Cl^-$ present at 199 eV in $KClO_4$ was measured to be less than one atomic percent. One will note that as the time of x-irradiation exposure increases, the amount of $KClO_4$ decreases with the corresponding increase in the amount of $Cl^-$. In fact after ∿2 hr of irradiation >10% $Cl^-$ in $KClO_4$ was found. Also a new peak can be seen at ∿206 eV, which is characteristic of the presence of $ClO_3^-$.

It is tempting to conclude from this above data that since $KClO_4$ photodecomposes almost immediately upon irradiation with soft x-rays of energies of <1500 eV (photons of $MgK_\alpha$ ∿1250 eV), there is an inherent problem with the XPS technique in the determination of $Cl^-$ concentrations in pyrotechnic blends containing $ClO_4$ oxidizers. A similar result was obtained by Copperthwaite and Lloyd for XPS studies of radiation [13]. They measured the decomposition kinetics of $NaClO_4$ under $AlK_\alpha$ irradiation.

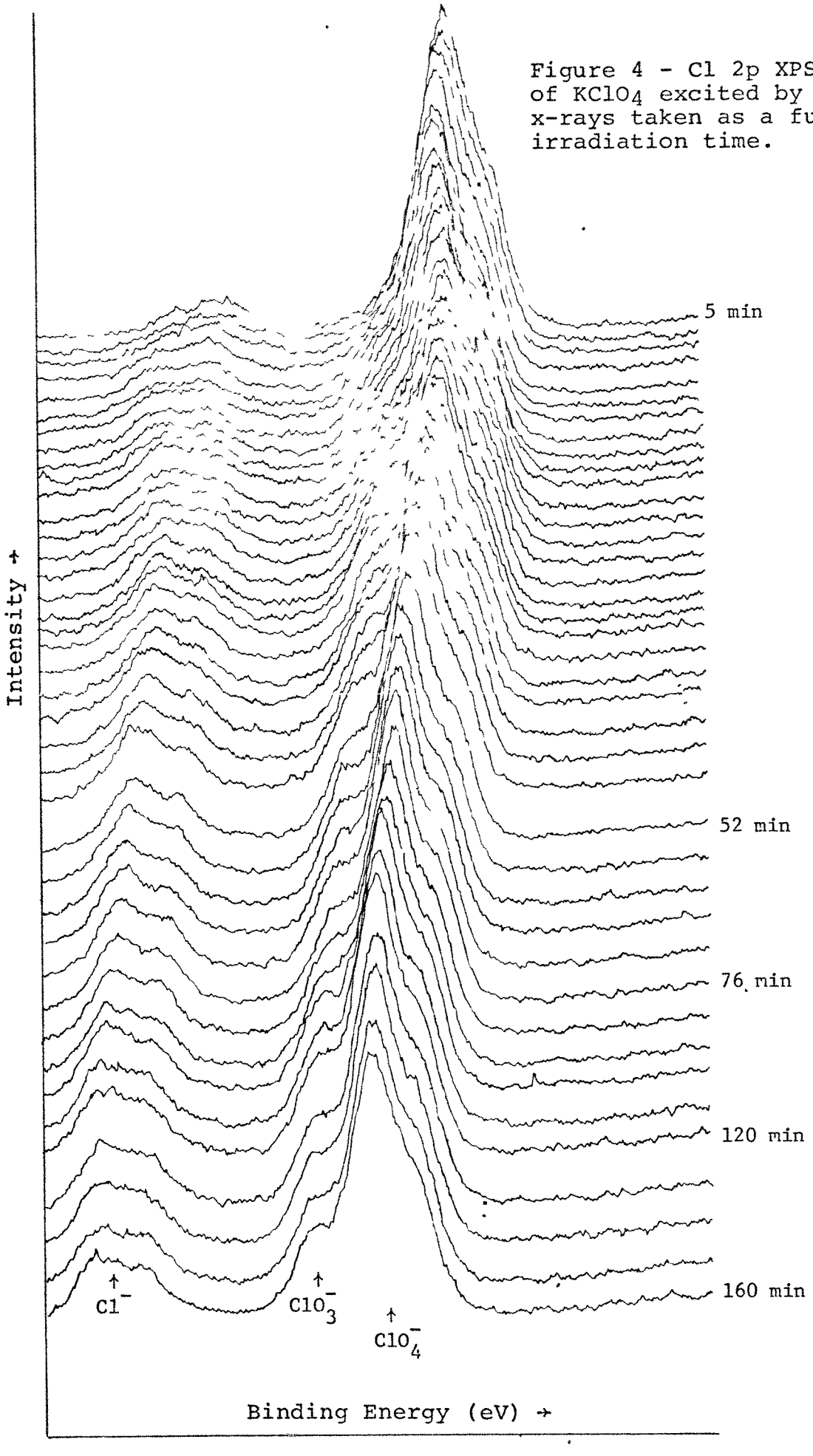


Figure 4 - Cl 2p XPS spectra of $KClO_4$ excited by Mg $K_\alpha$ x-rays taken as a function of irradiation time.

More recently at Mound we have measured the XPS chlorine 2p spectra of $KClO_4$ under irradiation with $MgK_\alpha$, $AlK_\alpha$, $TiK_\alpha$ and monochromatized $AlK_\alpha$ [10,11]. Monochromatized $AlK_\alpha$ is simply generated by passing $AlK_\alpha$ radiation through a quartz crystal monochromator [14]. Figure 5 shows the XPS spectra of $KClO_4$ exposed to monochromatized $AlK_\alpha$ for 15 minutes and for 15 hours [10,11]. No difference can be detected in the spectra of short and long exposure times. From these data we can conclude $KClO_4$ does not photodecompose under $AlK_\alpha$ x-ray energy photons contrary to Copperthwaite and Lloyd's results. The reason for photodecomposition of $KClO_4$ under non-monochromatized $AlK_\alpha$ has not been determined; however, it has to be due to (1) high energy Bhremsstrahlung which is not present in chromatized photons, and/or (2) infrared heating from the closeness of the x-ray tube. The Bhremsstrahlung radiation is removed by the monochromator and the infrared radiation flux is also reduced substantially because the filament heating source is far removed from the $KClO_4$ specimen. These results have been discussed in more detail elsewhere [10,11].

4. Al/$Cu_2O$ Pellets

In thermite studies at Mound, [2-5,9] it has been established that aluminum powders from the manufacturer have a layer of oxide on the particle surface. This surface oxide increased by approximately 20% after simply mixing at room temperature with the $Cu_2O$ oxidizer [2,3]. Pressing of this mixture for 15 min at 425°C has been shown to double the aluminum oxide surface thickness on the aluminum fuel [2,3]. It has also been established that the $Cu_2O$ is contaminated with a thin coating of CuO that disappeared upon heating [4,5]. The data which

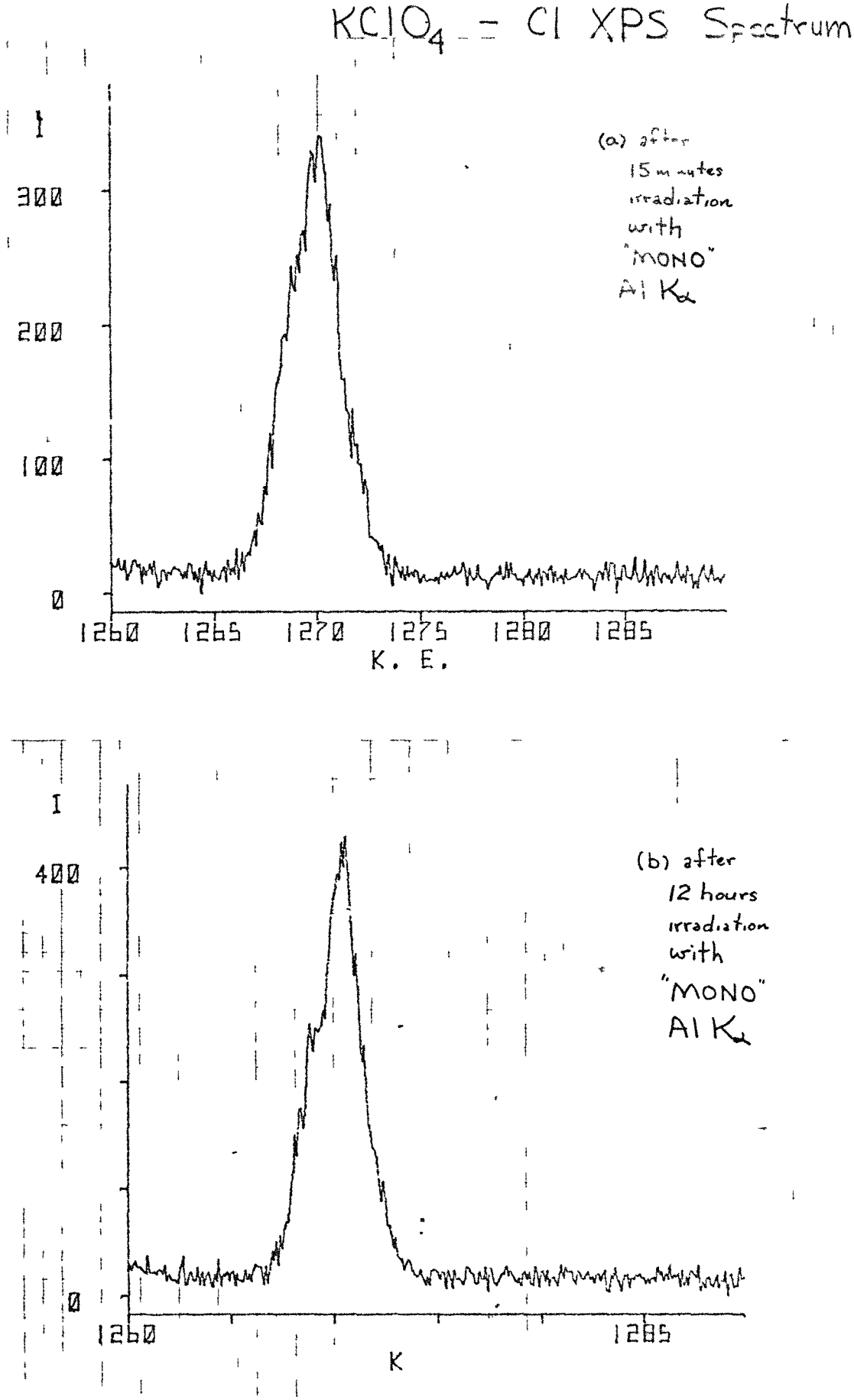


Figure 5 - Cl 2p XPS spectra of $KClO_4$ excited by monochromatized Al $K_\alpha$ irradiation for: (a) 15 minutes and (b) 12 hours.

follow show scanning Auger results taken on the interfacial region between the aluminum and $Cu_2O$ in the pressed pellet [9].

Figure 6 shows a secondary electron image of the outer surface of the $Al/Cu_2O$ pellet amplified some 1000 times; note that the grains of aluminum and $Cu_2O$ can be clearly observed. A wide beam Auger electron spectrum of this surface is shown in Figure 7. The data in Figure 7 clearly show the presence of the surface contaminants: chlorine, carbon, and sodium. From the observed pattern of the aluminum K-LL Auger spectrum, one can conclude that the surface aluminum is an oxide of aluminum. Also, the aluminum/copper signal ratio is larger than expected from the stoichiometric mixture. This measured ratio is in agreement with previous XPS data not discussed in this text [2,3].

Figure 8 shows the Auger outer surface maps of carbon, aluminum, and copper. The lighter areas signify an enriched area of the specific element. These data indicate that the surface of the pellet consists mainly of aluminum; this is due to the low surface tension of aluminum at 425°C as compared to $Cu_2O$ or copper metal. The surface tension is the measure of the work (or energy) required to create a fresh surface. A total component distribution of the surface can be easily constructed from the combination of the three spectra.

A three-dimensional analysis can be accomplished by sputtering while simultaneously Auger analyzing the remaining surface. The Auger electron in-depth elemental and chemical profiles (IDECP), shown in Figure 9,

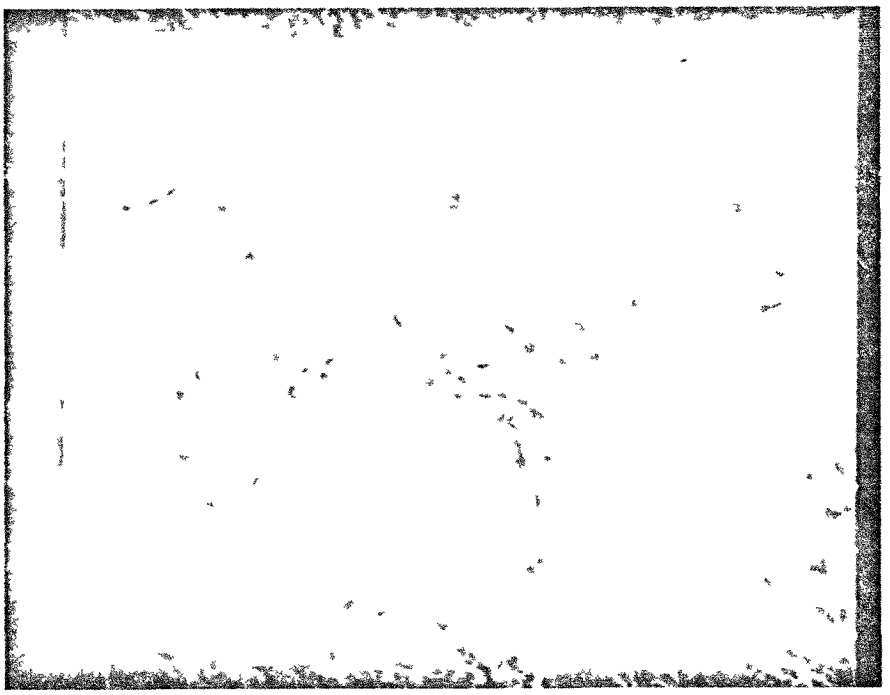

Figure 6 - Scanning electron image of $Al/Cu_2O$ pellet.

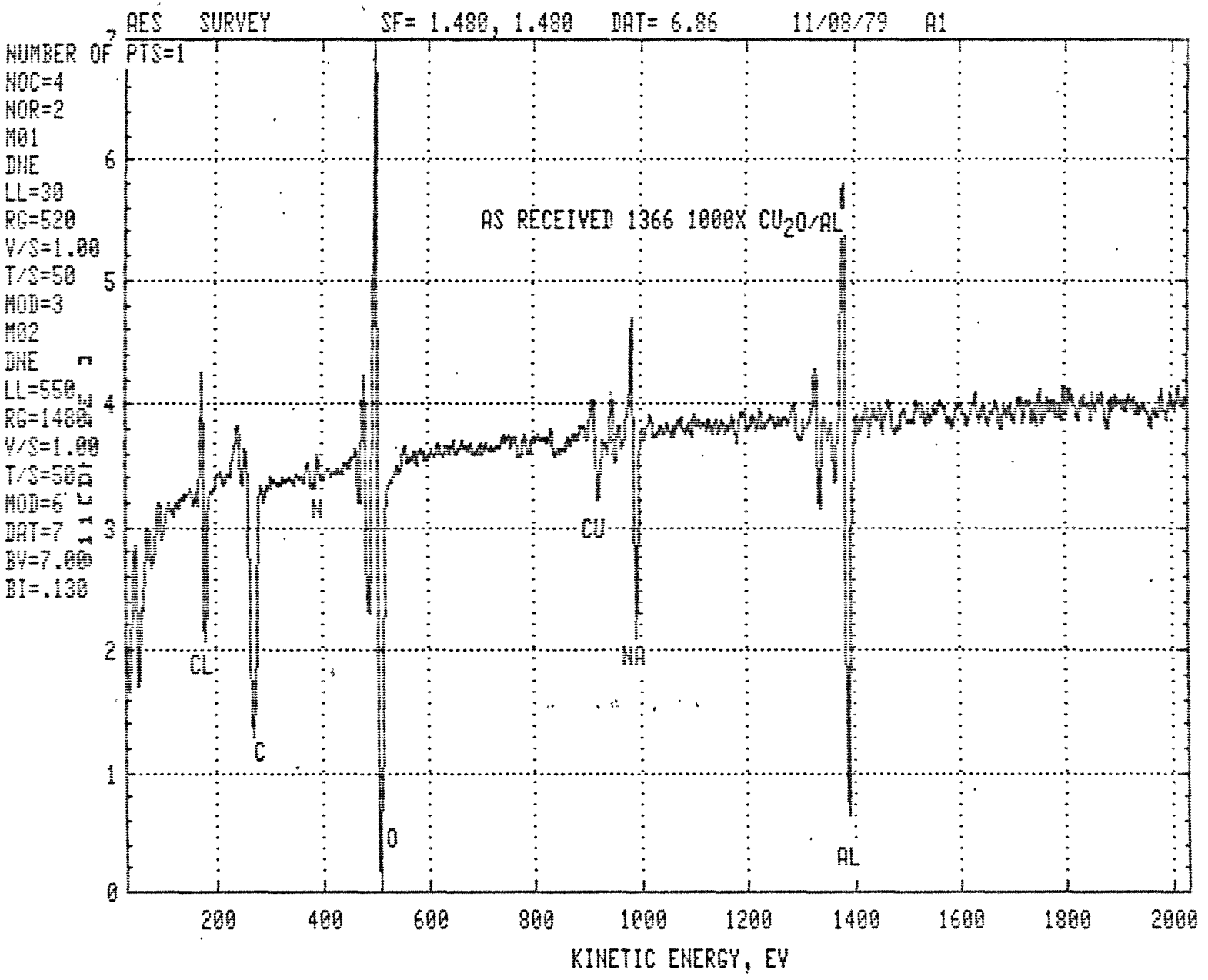


Figure 7 - A wide beam Auger electron spectrum at the surface of an Al/$Cu_2O$ pellet (1000X).

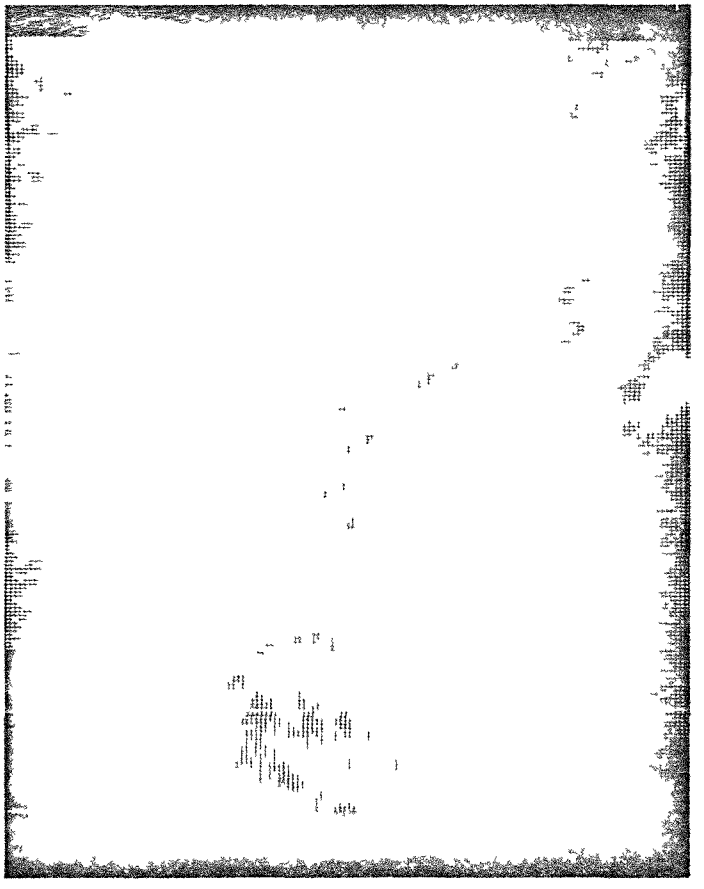


Figure 8 - Auger maps of outer surface of Pellet: (a) carbon, (b) aluminum, and (c) copper.

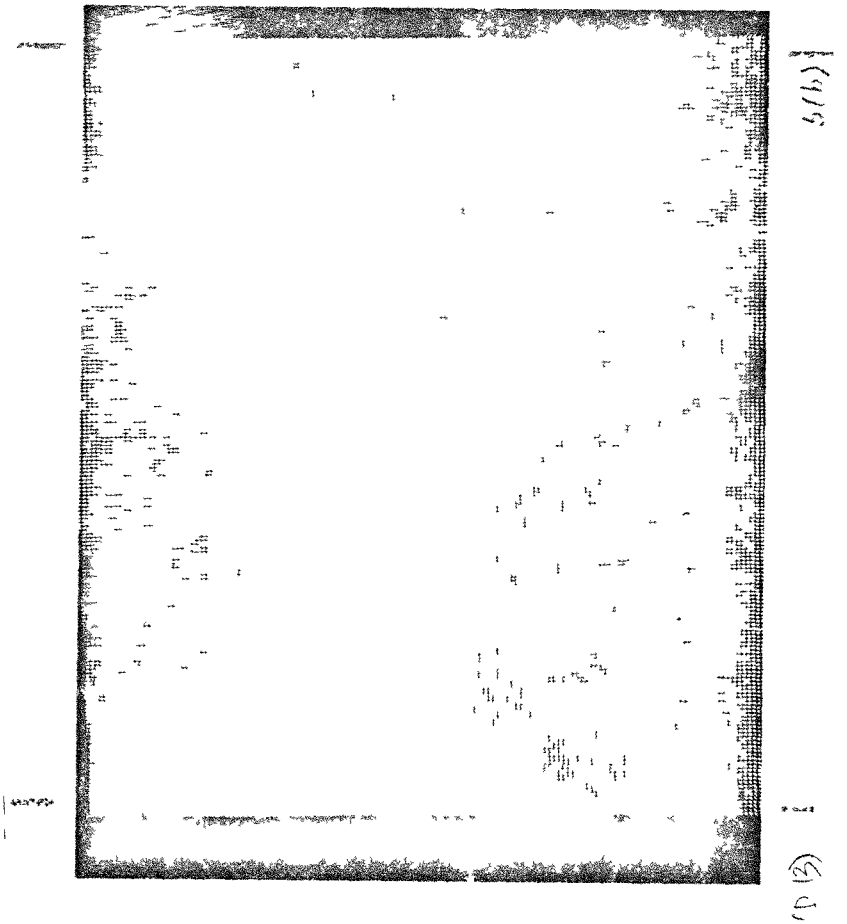

10000X AH AUGER M.P ≈ 1 MICRON (1)

(b)

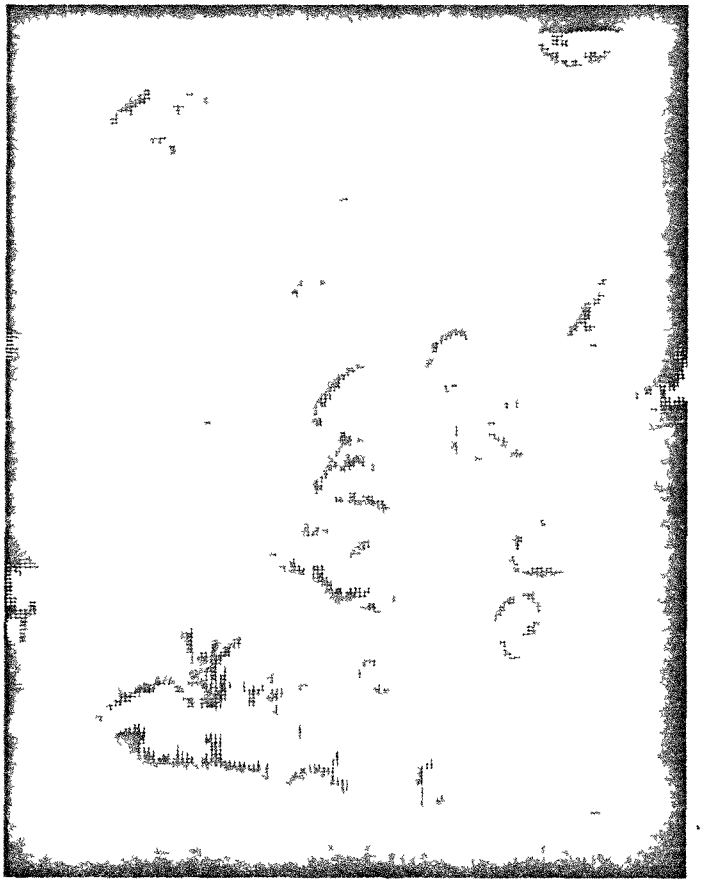

5(1)1

1000X Cu 920 eu Auger Map
1366 1 micron

(c)

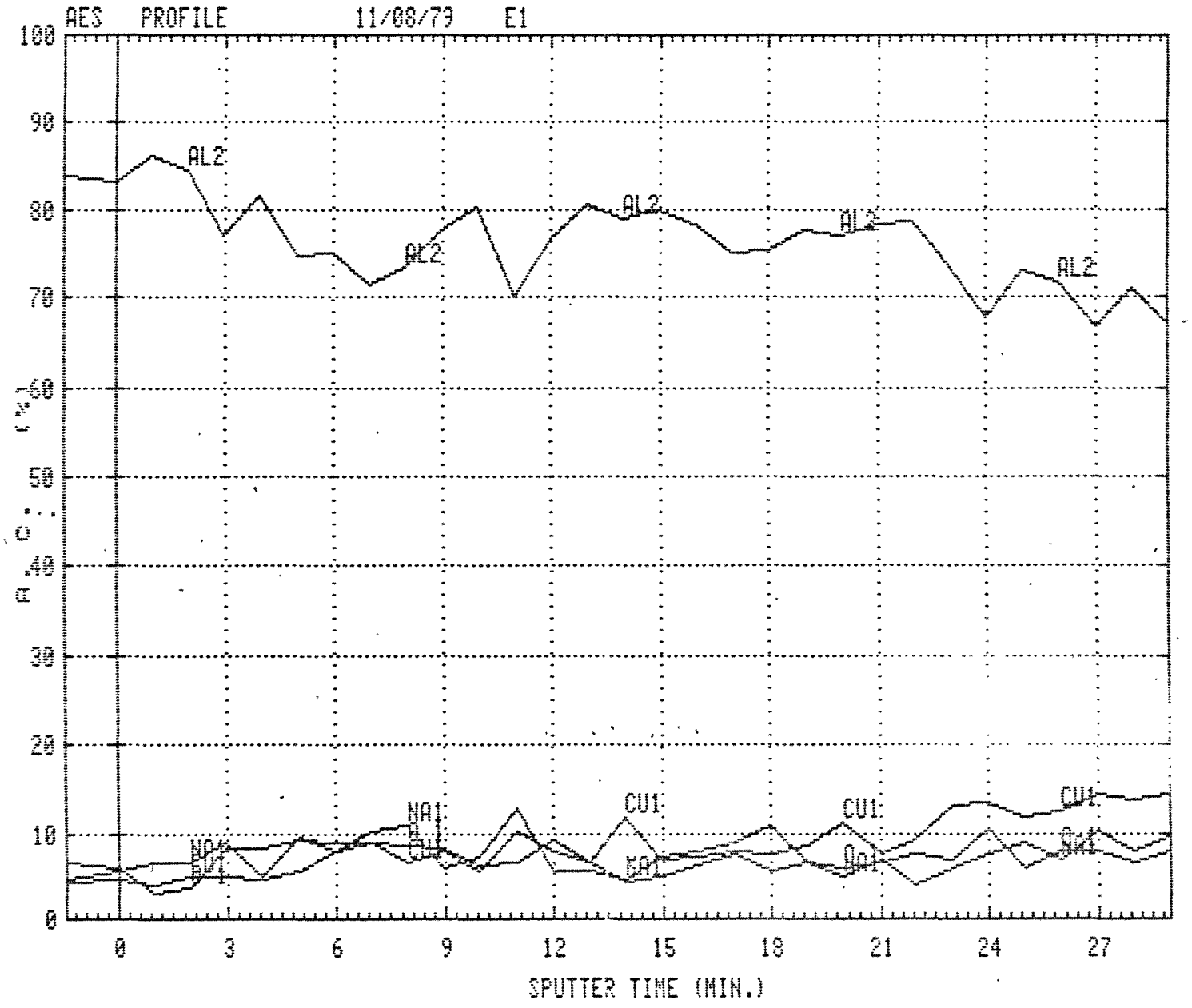


Figure 9 - Auger electron spectroscopic profile of an aluminum rich area in pellet.

illustrate that an aluminum rich spot is about 80-85 at. % aluminum and about 6-10 at. % copper. After sputtering has been applied at a rate of ~50Å/min, however, one will note a decrease in aluminum and an increase in copper. These data hint that under the enriched aluminum surface layer, there exists a stoichiometric cuprous oxide particle and that the thickness of the surface-enriched layer of aluminum is >1000Å.

A scanning electron micrograph of a fractured surface of another pellet is shown in Figure 10, and copper and aluminum Auger maps are illustrated in Figure 11. Auger electron spectra of Point 1 and Point 2 illustrate the presence of a $Cu_2O$ particle. Analysis of Point 2 following removal of 100Å shows the coexistence of aluminum and copper oxides, with a continuously increasing copper signal. This is clearly shown in Figures 12. This analysis suggests that there is a layer of the mixed or reacted aluminum and $Cu_2O$ surrounding a large grain of $Cu_2O$.

Thus, we have verified in this study that (1) the enriched-aluminum surface layer of a pressed pellet is >1000Å thick, and (2) an interfacial region is formed between the aluminum metal and the cuprous oxide during the hot-pressing operation. This interfacial region measured at least 100Å in thickness.

B. Explosive and Composite Explosives

Interest is increasing in the development of new plastic bonded explosive (PBX) materials for flying plate detonator applications. One of the advantages of a PBX is an improved mechanical strength of the powders and thus a better rigidity of the pellets into which the powders are pressed.

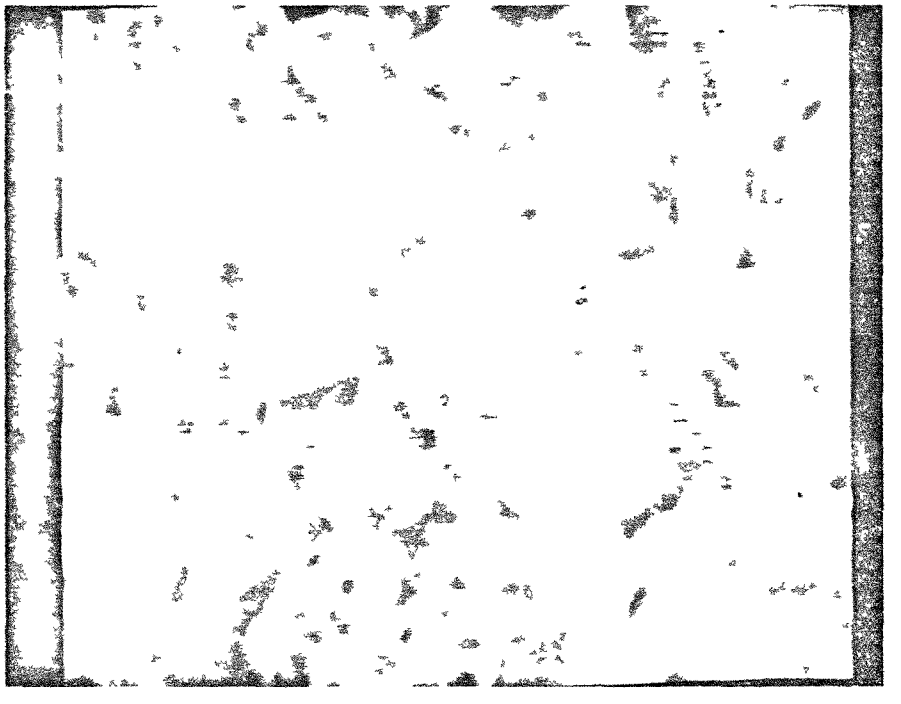

Figure 10 - Scanning electron micrograph of fractured surface of $Al/Cu_2O$ pellet (3000X).

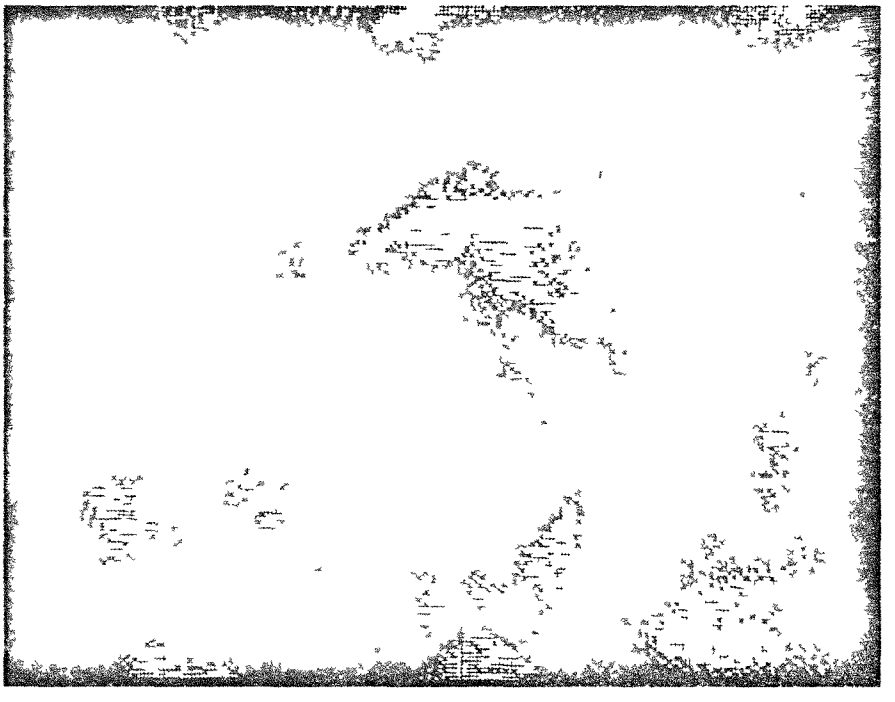

Figure 11 - Computer enhanced Auger maps of fracture surface of (a) copper and (b) aluminum.

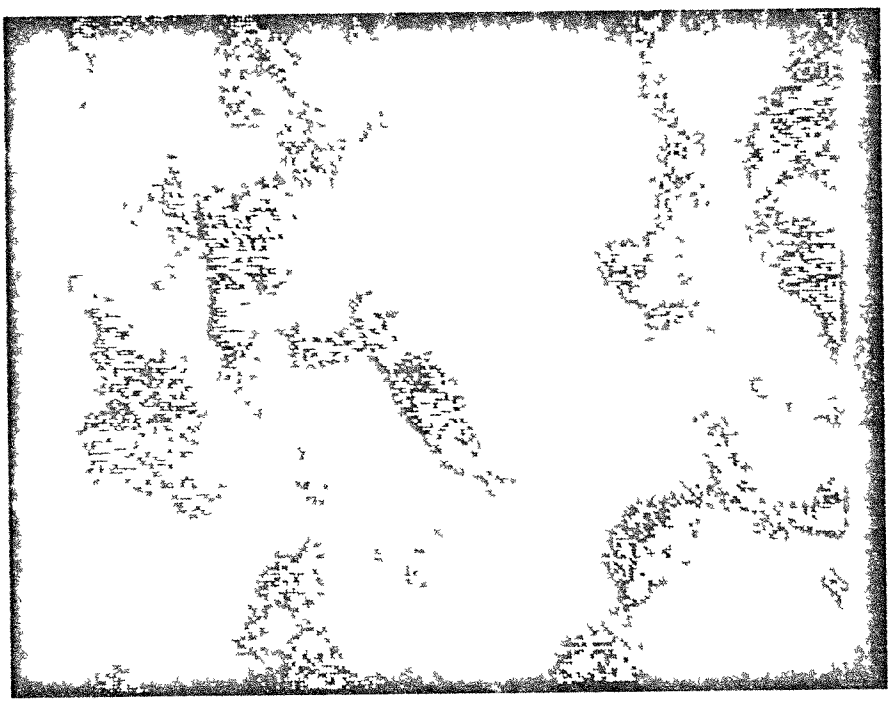

(b)

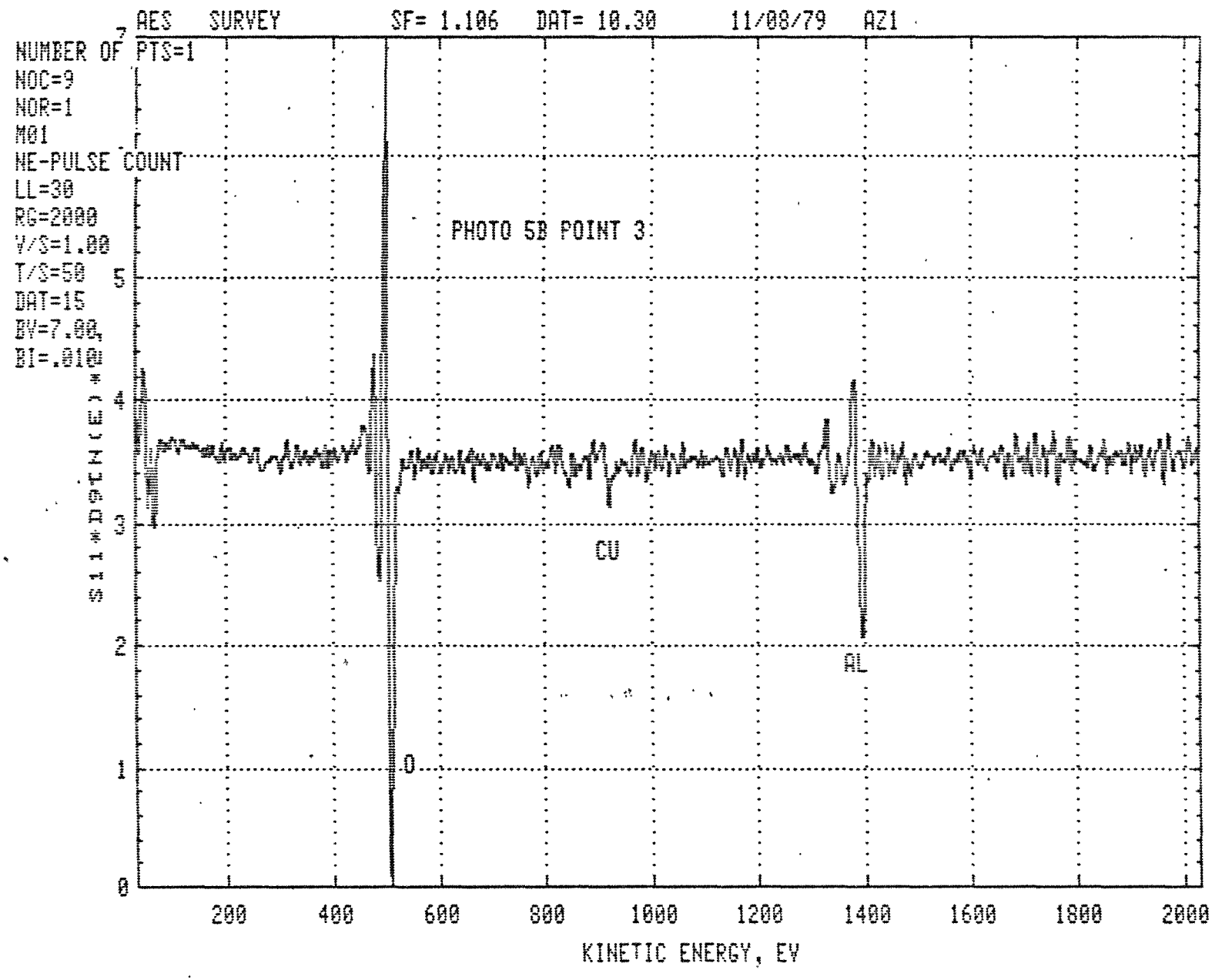


Figure 12a - Auger electron spectra of area rich in $Al_2O_3$, surface.

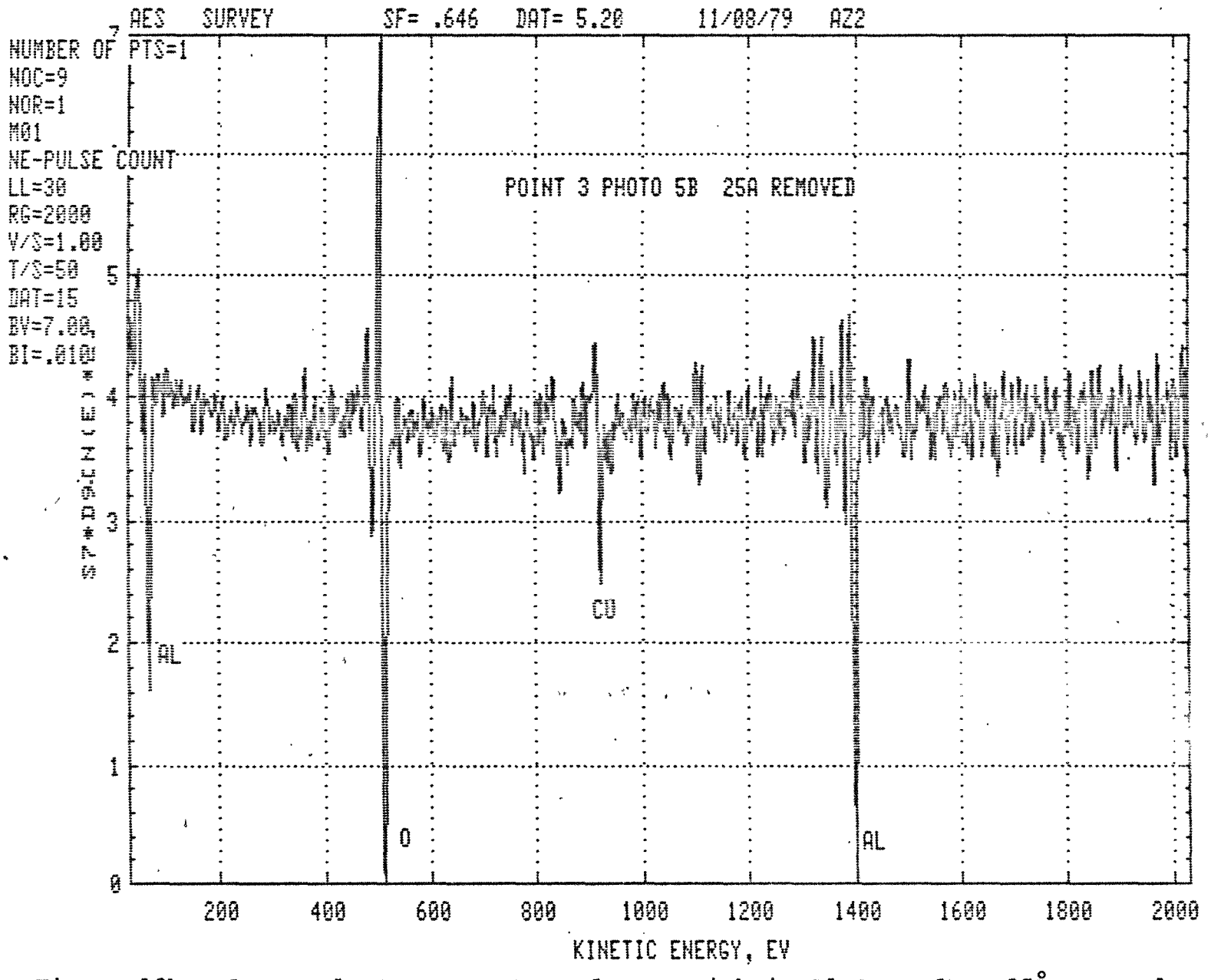


Figure 12b - Auger electron spectra of area rich in $Al_2O_3$, after 25Å removal.

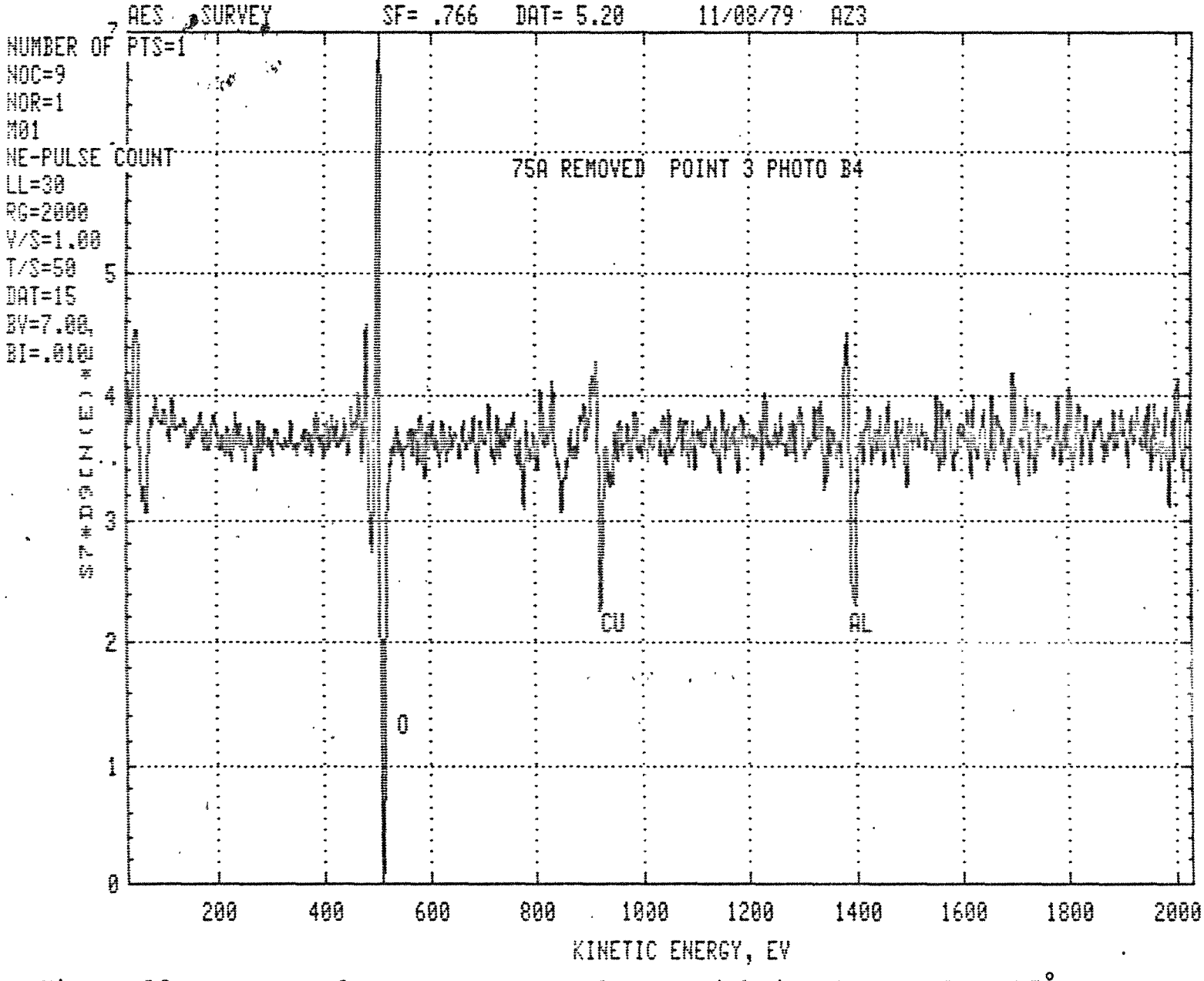


Figure 12c - Auger electron spectra of area rich in $Al_2O_3$, after 75Å removal.

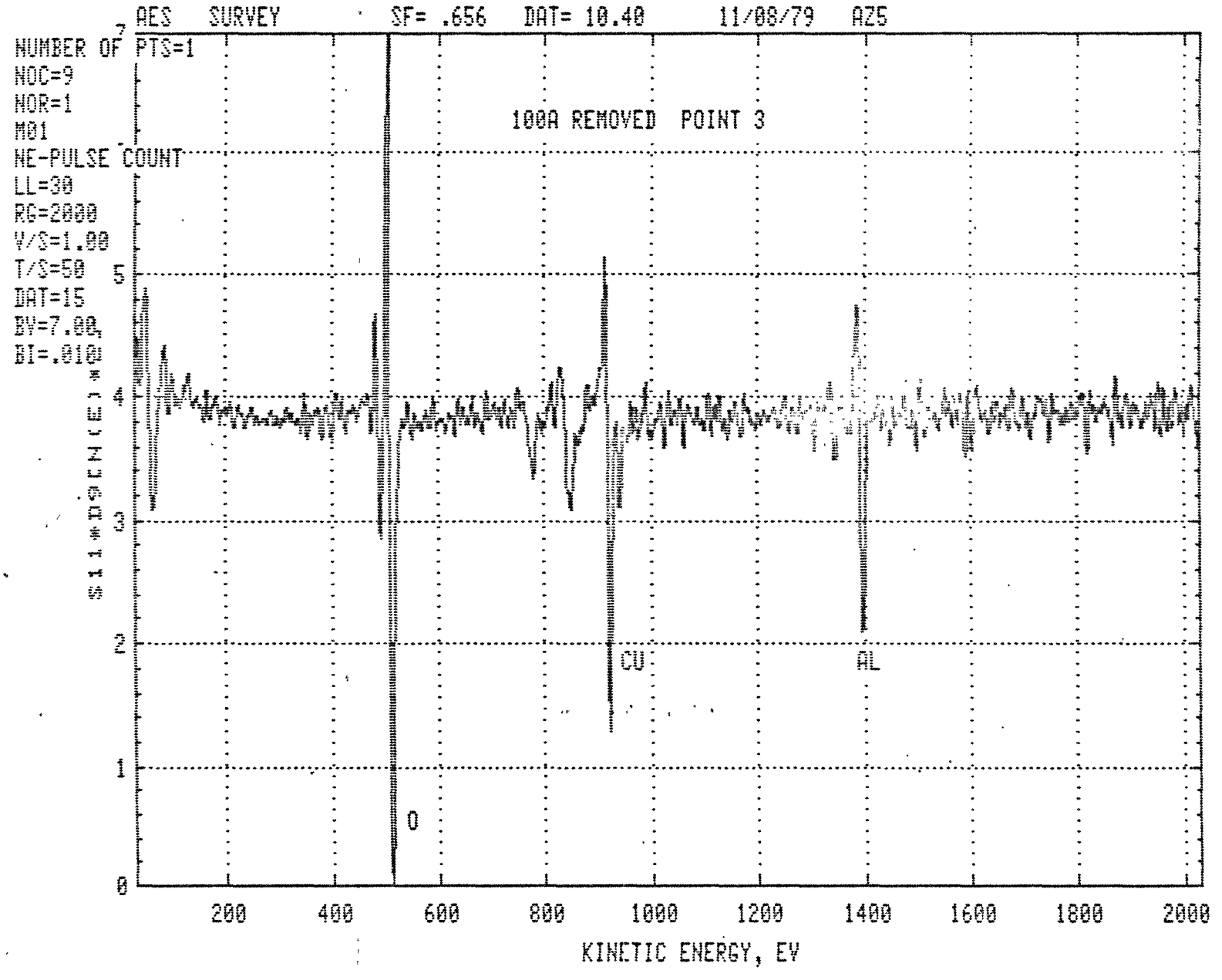


Figure 12d - Auger electron spectra of area rich in $Al_2O_3$, after 100Å removal.

The surface characteristics of two PBX materials, namely, a batch of PBX-9407 and a batch of LX-16, were evaluated with XPS and ISS. Both products contain a copolymer of vinyl chloride-chlorotrifluoroethylene. The type of explosive and content is different. To date, very little work has been done in using XPS to characterize either solid explosive reactants or composites. Some studies that have been accomplished at the Mound Facility are discussed in the following paragraphs.

Studies on the surface characterization of explosives, coatings and composites have been obtained on RDX, Exon-461 and PBX-9407, respectively. PBX-9407 is 94 wt % RDX coated with 5 wt % Exon. RDX and Exon have the following structures:

RDX =

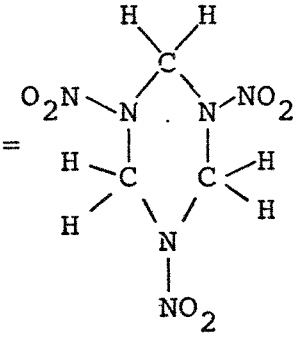

EXON =

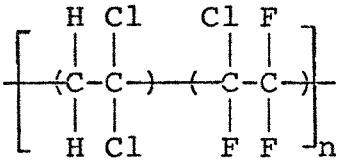

The high resolution elemental XPS spectra of F 1s, Cl 2p, N 1s and C 1s were recorded on each of the three samples (Exon, RDX and PBX-9407). Representative spectra of the four different elements are shown in Figure 13. No N signal was observed from the Exon and PBX samples; however, C, Cl and F intensities were identified. As expected no Cl and F peaks were seen with the RDX sample. From this qualitative information we can conclude that the substrate explosive particulate (RDX) in the PBX-9407 material was well coated. If we assume that the mean free path of photoelectrons in organic materials

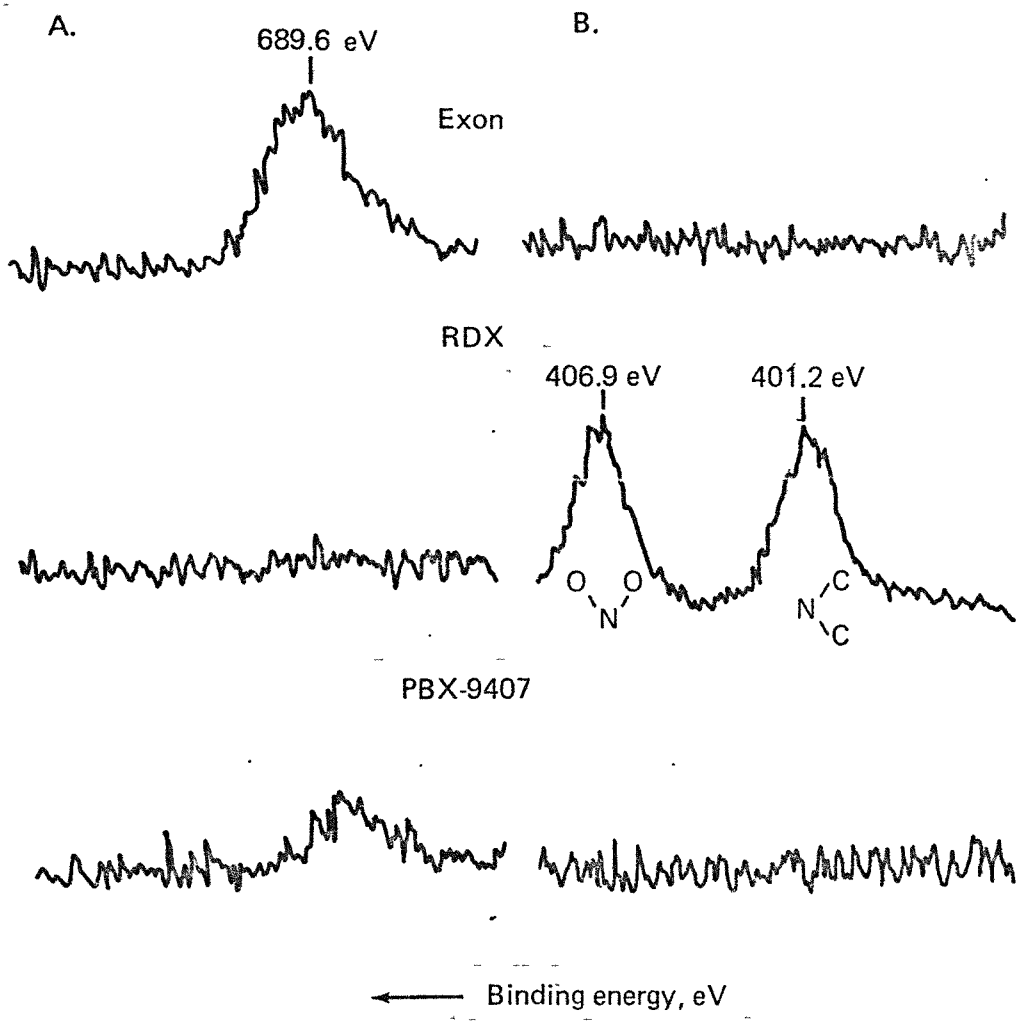


Figure 13 - XPS spectra of (a) F 1s, (b) N 1s, (c) C 1s and Cl 2p from EXON, RDX and PBX-9407.

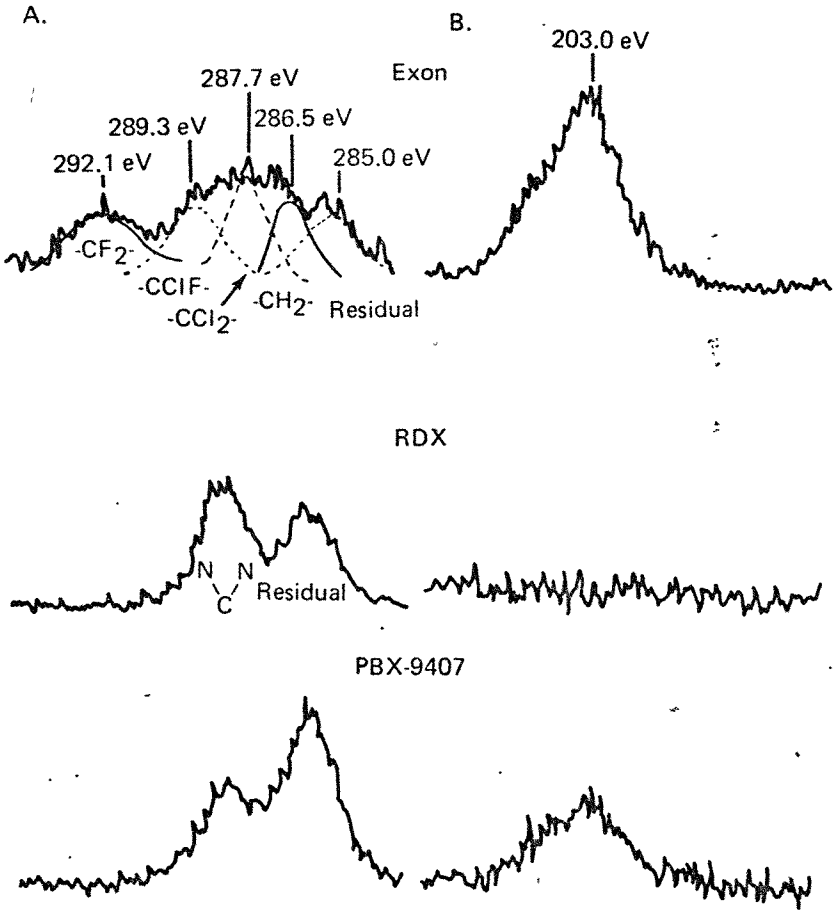


Figure 13 - Continued.

is <100Å° [14], and since no N 1s signal could be observed with this PBX, the coating on RDX in this PBX sample is >100Å. Table I summarizes the F 1s, Cl 2p, C 1s and N 1s data.

The F 1s and Cl 2p binding energies in Exon and PBX-9407 samples are characteristic of organic fluorides and chlorides. The C 1s data for Exon-461 are explainable in terms of its known molecular structure. However, in the PBX-9407 material, a different C 1s spectrum was observed (see Figure 13d). This suggests that the coating is not simply Exon.

Illustrated in Figures 14a, 14b, and 14c, respectively, are the overall C 1s and N 1s ESCA spectra of PETN and of coated PETN, LX-16. The LX-16 is 95 wt % PETN and 4 wt % Exon. These data indicate that the Exon coating on LX-16 is <100Å thick mainly because of the observation of the N 1s signal. Note also the presence of two N 1s ESCA peaks for the LX-16 sample (Figure 14b). The higher binding energy peak is assigned to nitrogen-bound-to-oxygen atoms, such as in the $ONO_2$ group, but the origin of the lower binding energy species is not clear at this time.

With ion scattering spectroscopy (ISS) one is able to determine the composition of just the outermost atomic layer of a sample surface. The ISS data given in Figure 15 are representative of one: (a) 2-min, (b) 12-min, and (c) 45-min $^3He^+$ exposure. In all cases, the elements fluorine, oxygen and nitrogen were detected initially. Exposing for longer periods of time did not change the relative amounts of these elements appreciably. The scan taken after 45 minutes of exposure did show a slight increase in the carbon energy region. The initial detection of N signal in the coated powder likely suggests that the

Table I

ESCA DATA ON EXON, RDX, AND PBX-9407

| Element and Level | Identification | EXON B.E. | EXON Atoms F - 100 | RDX B.E. | RDX Atoms F - 100 | PBX-9407 B.E. | PBX-9407 Atoms F - 100 |
|---|---|---|---|---|---|---|---|
| F 1s | C-F (organic fluorine) | 689.6 | 100 | --- | --- | 689.3 | 100 |
| Cl 2p, | C-Cl (organic chloride) | 203.0 | 105 | --- | --- | 202.6 | 70 |
| N 1s | 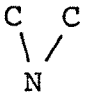 | --- | --- | 401.2 | --- | --- | --- |
| | 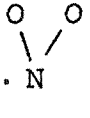 | --- | --- | 406.9 | --- | --- | --- |
| C 1s | C-C (residual) | 285.0 | 71 | 285.0 (residual) | | 285.0 | 215 |
| | $-CH_2-$ | 286.5 | 92 | --- | --- | 286.0 | 776 |
| | $-CCl_2-$ | 287.7 | 121 | 287.7 (N-C-N) | --- | 287.0 | 823 |
| | -CClF- | 289.3 | 83 | --- | --- | 288.5<br>289.8 | 537<br>477 |
| | $-CF_2-$ | 292.1 | 67 | --- | --- | --- | --- |

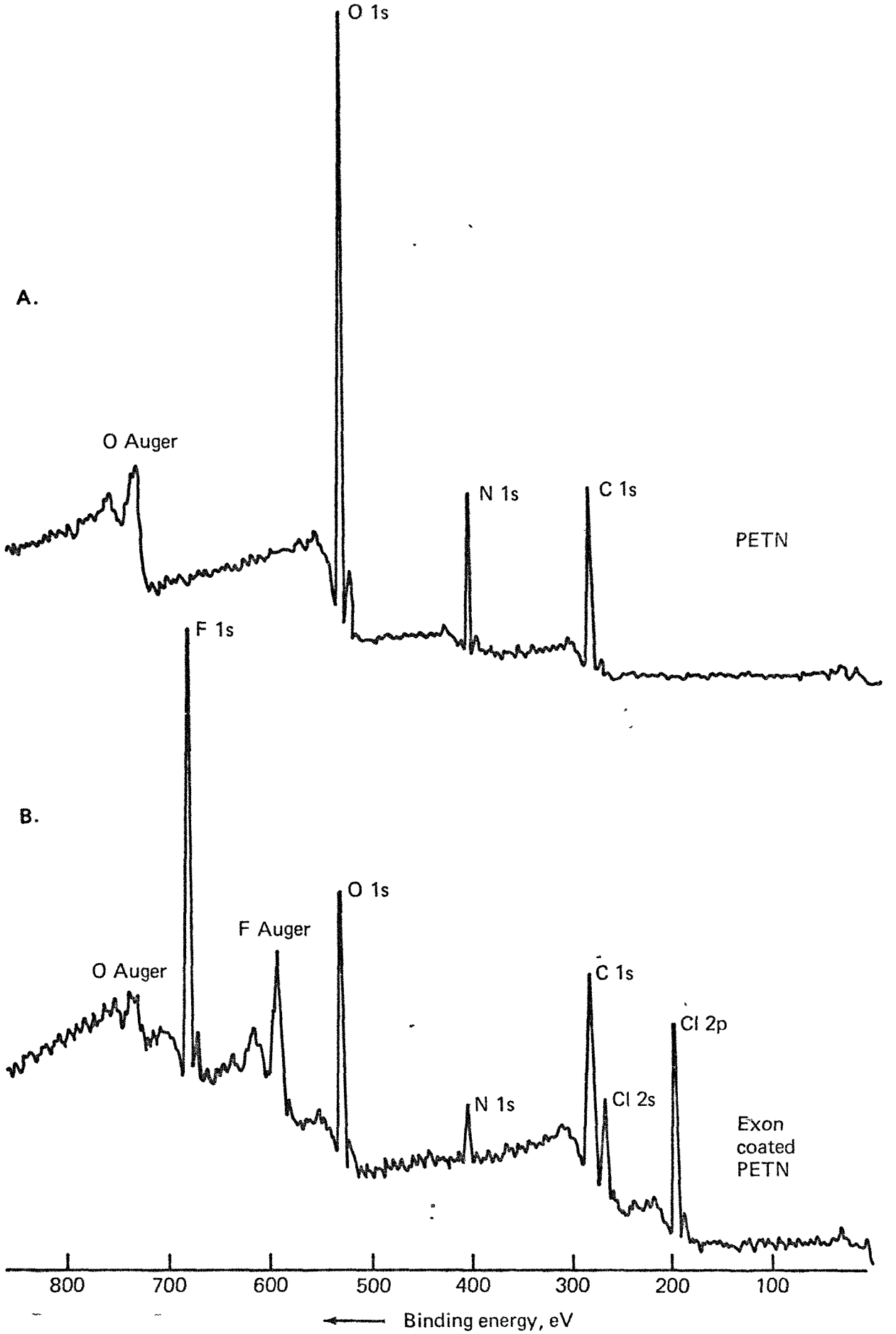


Figure 14 - XPS spectra of (a) overall, (b) C 1s and N 1s from PETN and LX-16.

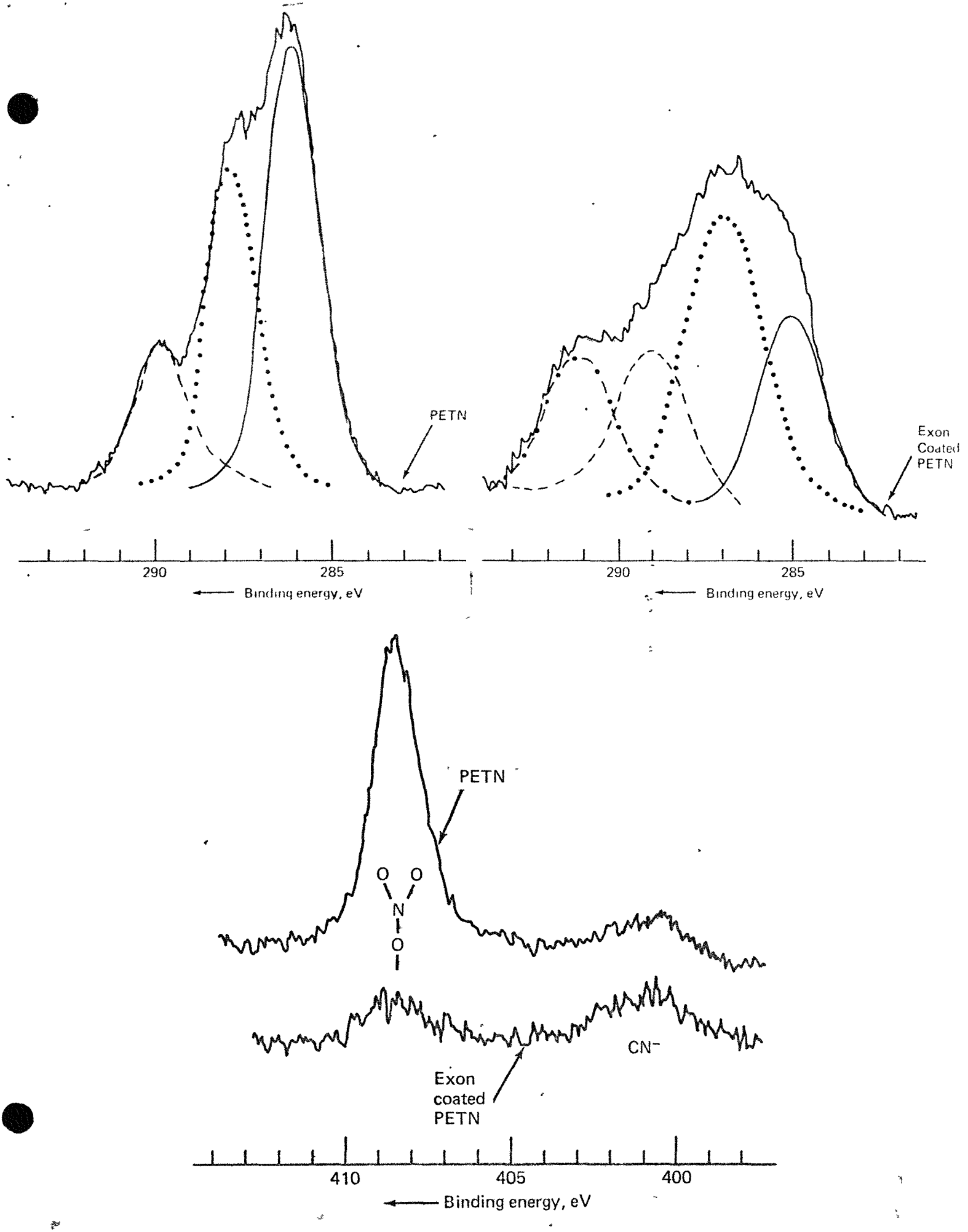
PETN
290
285
Binding energy, eV
Exon
Coated
PETN
290
285
Binding energy, eV
PETN
O
O
N
O
CN⁻
Exon
coated
PETN
410
405
400
Binding energy, eV

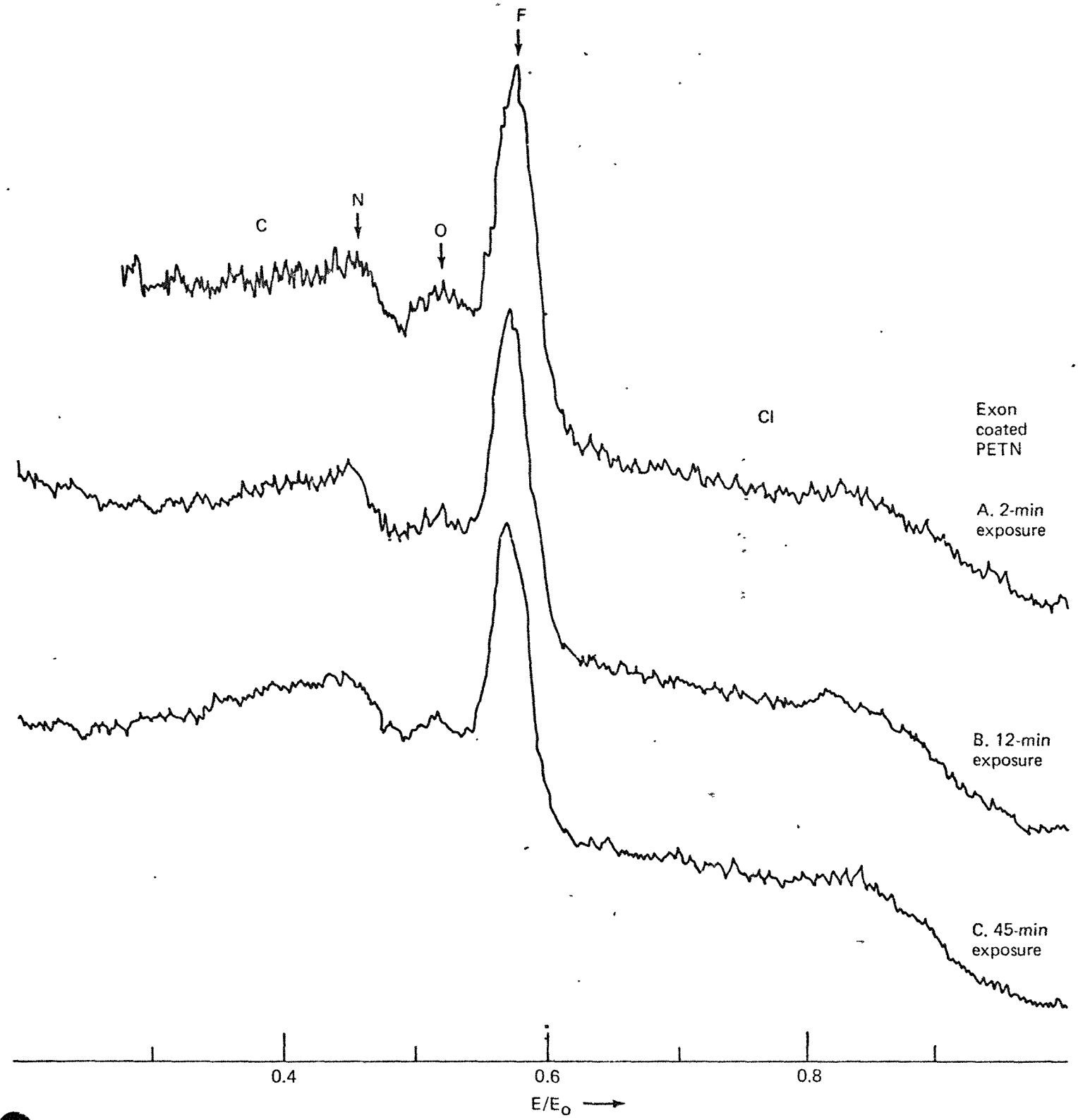


Figure 15 - ISS spectra of LX-16 after (a) 2 minutes, (b) 12 minutes and (c) 45 minutes sputtering by $^3He^+$.

surfaces of PETN powders are not completely coated with Exon 461, possibly due to the low percentage of coating material used (only 4%).

There are a couple of points about the data which are not explained. First, chlorine was detected using ESCA, yet it was not detected with ISS. It should appear at $E/E_o = 0.74$. Also, very little carbon was detected with ISS. It could be that these elements actually are not present in the first few monolayers, although this does not seem likely.

From the ISS data for the LX-16 sample, it can be concluded that the coating on the PETN particles is not uniform and is, in fact, absent in some regions. This is in agreement with the ESCA results discussed above.

Consequently, we can conclude that in PBX-9407, the surface coating is complete and $\geq$100Å; but in LX=16, the coating is $<$100Å or even incomplete.

C. Compatibility

We have not done any controlled experiments of examining for possible changes in the surface chemistry of HE materials with their containment due to particle-container interaction. We have, however, shown the effect that cleaning (solvent and argon plasma) and oxidation ($H_2O_2$ and $O_2$ plasma) have on the surface chemistry of iron-nickel 50-50 alloy [15]. Specifically, AES was used to determine the relative composition and thickness of oxide films following one of several of the surface treatments.

The results of these cleaning and oxidation studies are summarized in Table II. It can be seen from the data that the nickel-to-iron ratio is significantly lower for the peroxide-cleaned and $O_2$ plasma-cleaned samples as compared with the other four treated specimens.

Table II

AUGER PEAK HEIGHT RATIOS
DETERMINED FROM SURFACE SCANS

| Sample Treatment | C/Fe | O/Fe | Ni/Fe |
|---|---|---|---|
| Ultrasonic, 2 min in methanol | 1.4 ± 0.4 | 3.6 ± 0.4 | 1.8 ± 0.1 |
| Ultrasonic, 15 min in methanol | 1.4 ± 0.1 | 3.0 ± 0.1 | 1.7 ± 0.1 |
| Ultrasonic, 15 min in PCE | 1.4 ± 0.1 | 2.5 ± 0.2 | 1.5 ± 0.1 |
| $O_2$ plasma, 15 min at 100 watts | 1.1 ± 0.1 | 4.3 ± 0.1 | 0.56 ± 0.02 |
| Ar plasma, 15 min at 100 watts | 1.5 ± 0.1 | 5.0 ± 0.1 | 2.0 ± 0.1 |
| 15% $H_2O_2$, 24 min | 1.3 ± 0.1 | 3.4 ± 0.1 | 0.68 ± 0.02 |

Also, the carbon-to-iron is lower for the peroxide-cleaned and the $O_2$ plasma-cleaned samples.

Depth profiles of each of the samples (six) have been generated. Figure 16 gives the profiles of the $O_2$ plasma-cleaned foil, the peroxide-cleaned foil, and the foil which was ultrasonically cleaned for 15 minutes in methanol. In order to objectively compare the thicknesses of the oxide layers on the foils studied, the sputtering time required to reduce the oxygen peak to 50% of its maximum intensity, $O_{50\%}$, was determined from the depth profiles. Similarly, the sputtering time required to reduce the carbon to 50% of its maximum intensity, $C_{50\%}$, was determined for each of the foils. The values of $O_{50\%}$ and $C_{50\%}$ are given in Table III. Each entry in this table is the average of three independent measurements. From the table it can be seen that $O_{50\%}$ is highest for the $O_2$ plasma-cleaned sample. Also, $C_{50\%}$ is lowest for this sample.

From the surface nickel-to-iron ratios and the depth profiles it can be seen that for the $O_2$ plasma-cleaned and the peroxide-cleaned samples, both of which have comparatively thick oxides, there is a surface enrichment of iron or a surface depletion of nickel. For the samples cleaned in methanol or PCE, the surface nickel-to-iron ratio is very close to that in the bulk, which was measured to be 1.5. The lower carbon levels measured on the peroxide-cleaned and $O_2$ plasma-cleaned samples indicate that these samples have a reduced tendency to adsorb atmospheric hydrocarbons.

Thus, in this study we have shown that the iron-nickel foils cleaned in methanol or PCE have a surface Ni/Fe ratio which is close to the bulk value. On the $O_2$ plasma-cleaned and the

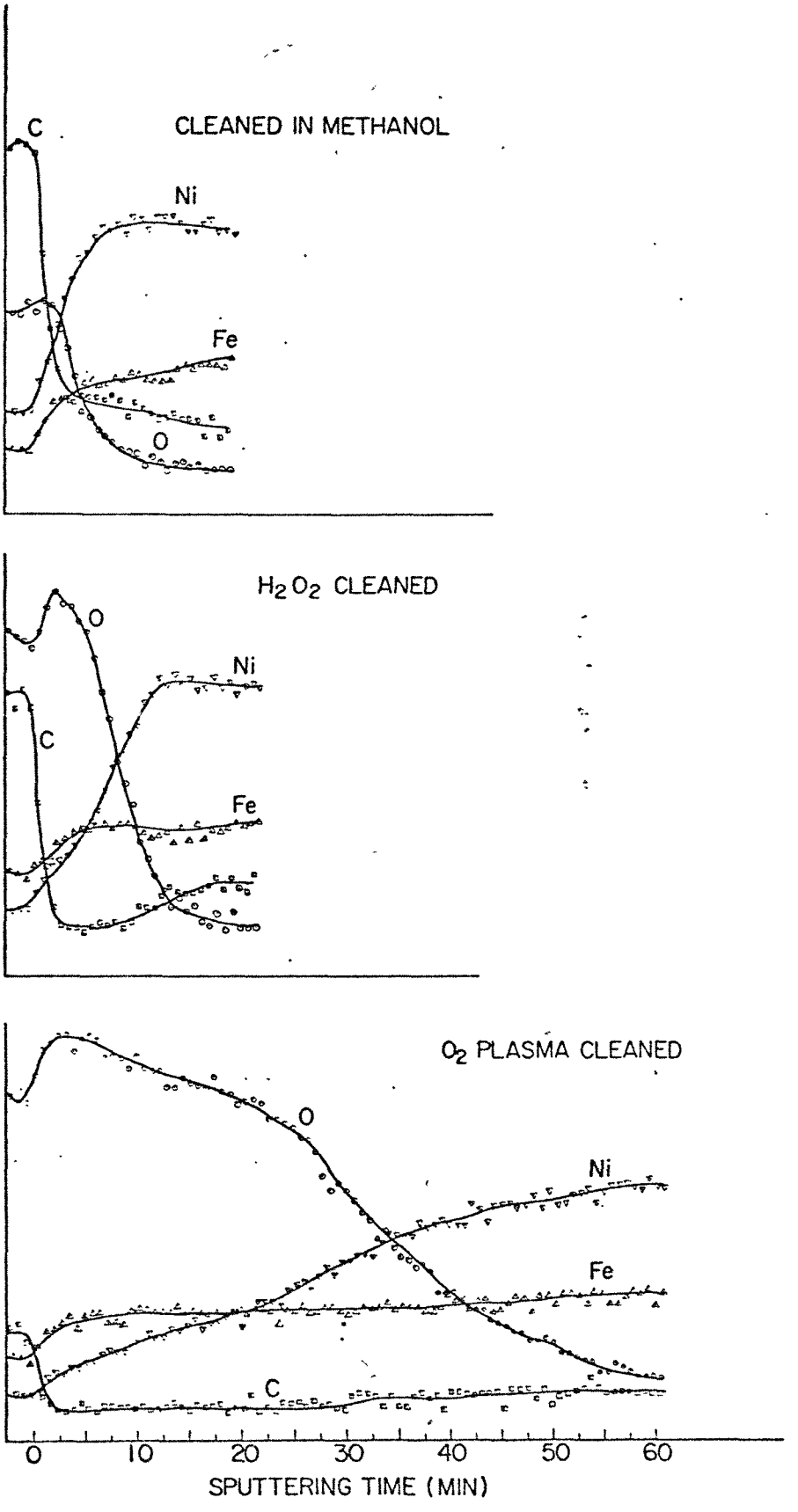


Figure 16 - Auger depth profiles of Fe-Ni foils having different surface treatments.

Table III

$O_{50\%}$ AND $C_{50\%}$ VALUES DETERMINED

FROM AUGER DEPTH PROFILES

| Sample Treatment | $C_{50\%}$ (minutes) | $O_{50\%}$ (minutes) |
|---|---|---|
| Ultrasonic, 2 min in methanol | 0.6 ± 0.1 | 3.1 ± 0.6 |
| Ultrasonic, 15 min in methanol | 1.3 ± 0.1 | 4.2 ± 0.2 |
| Ultrasonic, 15 min in PCE | 1.1 ± 0.1 | 4.5 ± 0.3 |
| $O_2$ plasma, 15 min at 100 watts | 0.5 ± 0.1 | 30.4 ± 3.8 |
| Ar plasma, 15 min at 100 watts | 0.6 ± 0.2 | 6.7 ± 1.3 |
| 15% $H_2O_2$, 24 min | 0.9 ± 0.1 | 8.1 ± 0.4 |

peroxide-cleaned foils, the surface Ni/Fe ratio is a factor of two to three lower than the bulk value. This indicates a significant iron enrichment in the surface oxide. The oxide thickness as a function of surface treatment was shown to increase in the following order: solvent cleaned < peroxide cleaned $<O_2$ plasma cleaned; the surface carbon levels were found to be the lowest on the $O_2$ plasma-cleaned and peroxide-cleaned samples.

## III. SURFACE ANALYSIS CAPABILITIES AT THE MOUND FACILITY

Chemical analysis of surfaces on the monolayer level has recently been attainable due to advances in instrumentation. Scanning Auger Electron Microscopy (SAM), X-Ray Photo Electron Spectroscopy (XPS) or Electron Spectroscopy for Chemical Analysis (ESCA), Secondary Ion Mass Spectroscopy (SIMS), and Ion Scattering Spectroscopy (ISS) are the most common surface analytical techniques that are used in material analysis. The Mound Facility will have available in FY 1981 all of the above techniques for solid surface characterization of almost any HE material. All of the techniques and equipment are discussed below.

### A. Scanning Auger Microscopy (SAM)

Auger electron spectroscopy involves a non-radiative decay of an inner-shell vacancy and is used as a technique for rapid qualitative and semi-quantitative analysis of solid surfaces. SAM involves the scanning of an electron beam in Auger excitation and simultaneously analyzing the Auger electrons. In the scanning mode elemental surface maps are obtained. Integrated with the SAM are: a low-magnification, secondary electron detector (SED); and an in-depth, elemental and chemical profiling (IDECP) capability. SED images allow areas of

interest to be pinpointed, then Auger analyzed with relative ease. The Auger/IDECP capability allows for rapid elemental and chemical profiling to be accomplished from the surface to the bulk.

The Mound Facility will have two SAM spectrometers available in FY 81, one a high resolution variety capable of obtaining detailed Auger surface spectra (Kratos X-SAM 800), and the second, a low resolution cylindrical mirror analyzer (CMA) model; the exact model of the low resolution CMA instrument has not been determined. The low resolution instrument will be primarily used for surface analysis of radioactive "HOT" specimens. The Kratos X-SAM 800 is fitted with a sub-micron electron gun capable of analyzing particles that differ in size by $\sim$1 micrometer. With the Kratos instrument the Auger or SAM images are obtained either in the analog or digital mode of operation. In the analog mode, Auger or SAM data are generated with exciting electron beam current densities of $\geq$0.5 $mA/mm^2$. This current density will cause thermodynamically unstable materials to decompose prior to or during analysis. In the case of explosives or composites of very unstable pyrotechnic blends, such as $B/Ca_2CrO_4$, this could be disastrous to the equipment. However, in the digital mode of Auger analysis where the data are time averaged and stored in a microprocessor, very low current densities are used, $10^{-3}$ less than the analog mode; therefore, with the Kratos instrument Auger analysis of explosives and composites is possible. In addition, the Kratos SAM is capable of analyzing up to 5000 eV electrons. Since higher kinetic energy electrons have greater mean free paths, it will be possible to analyze with this instrument subsurface Auger

electrons characteristic of the interface or bulk of a composite. This will be particularly beneficial in performing studies on binder-explosive interfaces.

The Kratos SAM is also fitted with a 3M mini II ion gun capable of generating IDECP profiles with argon ions at the rate of a few hundred Å/min. The Kratos instrument contains turbomolecular pumps and titanium sublimation and cyropumping in order to achieve ultra high vacuum conditions. A heating and cooling stage is also available. This pumping and stage combination will allow small quantities of HE materials to be heated to 1200°C or cooled to 90 K in situ during Auger analysis.

For Auger or SAM analysis of radioactive materials a CMA Auger spectrometer capable of focusing electrons with energies up to 10 keV will be used. The excitation beam will be capable of focusing to a 3-micron spot. The instrument will allow for the detection of all elements except hydrogen and helium with a sensitivity on the order of one atom in $10^3$ surface atoms. IDECP is available using a 2-3 keV Auger ion sputter gun and the presence of several elements can be monitored as the surface is sputtered away at rates of up to 200Å per minute.

B. X-Ray Photoelectron Spectroscopy (XPS)

The analytical technique XPS involves the interaction of x-ray photons having a constant energy, $h\nu$, with bound electrons in a sample, having a binding energy $E_B$. Via the photoelectric effect, these bound electrons are promoted into a continuum outside the sample as photoelectrons with a kinetic energy, $E_K$. By measuring the various values

of $E_K$ for photoelectrons ejected from a sample, one can determine by simple subtraction ($h\nu - E_K$) the binding energy $E_B$ for all the energy levels of atoms or molecules in the sample.

A qualitative analysis of the elements present on the surface is accomplished by measuring values of $E_B$ to within a few electron volts; the oxidation state of an element is characterized by determining $E_B$ to within a couple of tenths of an eV. Semi-quantitative surface atom concentrations are ascertained by measuring the photoelectron peak heights and adjusting for the sensitivity of the instrument to the different elements.

XPS analysis is to be obtained with the Kratos X-SAM 800 with an automated data collection microprocessor system. XPS measures the kinetic energy of x-ray excited photoelectrons. With the X-SAM 800 various x-ray sources such as Mg, Al, Si, Ti and Cu, are available which will allow for probing the surface, subsurface and bulk of pyrotechnics or composites with higher energy photons. The Kratos instrument is also fitted with an x-ray monochromator of proper design for monochromatizing $AlK_\alpha$ radiation. This x-ray source is imperative for $KClO_4$ to be examined in pyrotechnic blends, as described in the text, without causing perchlorate degradation.

C. Secondary Ion Mass Spectroscopy (SIMS)

An increasing interest in the analysis of material surfaces has led to the development of SIMS. SIMS analysis of a material is accomplished by bombarding a sample to be analyzed with a beam of 0.5 to 4 keV ions. These primary ions cause the outer atomic layers from 1 to 10Å of a material to be sputtered. A small fraction of the

sputtered species are ejected as positive or negative ions; however, most of the material leaves as neutral atoms or molecules. The sputtered surface ions are then extracted into a mass spectrometer for mass/charge separation to provide an analysis of that portion of the material sampled by the primary ion beam. It is the most sensitive of all the depth profiling methods and the most sensitive in determining small structure changes; however, it suffers from orders of magnitude variation in sensitivity from one element to the next.

The SIMS system at Mound consists of a Kratos mini I ion beam gun, as the excitation source, and a UTI Quadrupole Mass Spectrometer. The mini I ion beam gun is capable of $\sim$100$\mu$ spot size and raster gating for improved depth resolution and imaging. The UTI quadrupole has one amu mass resolution for low mass range between 1 and 300 amu. The Kratos equipment has both positive and negative mass analysis.

D. Ion Scattering Mass Spectroscopy (ISS)

Ion Scattering Spectrometry (ISS) is a simple method of performing surface analysis on the level of monolayer sensitivity. A beam of low-energy noble gas ions (such as helium, neon or argon) is used to bombard the surface of a sample. The energy distribution of the scattered primary ions is then measured with an electrostatic energy analyzer. For a fixed scattering angle, there is a simple, unique relationship involving the masses of the probe ion and the surface atom, and the energies of the probe ion before and after scattering. As a result, the energy distribution of the scattered ions is representative of the mass distribution of the surface atoms. The relationship between

scattered energy and intensity is straightforward, since each element is responsible for only one peak. ISS is perhaps the most surface-sensitive technique available, allows for true atomic monolayer identification to be made, and is the most quantitative surface analysis technique known. The 3M mini II ion gun on the Kratos instrument gives rise to the monoenergetic ions required for ISS, and the hemispherical electrostatic plates decode the kinetic energy of the scattering ions. Also available for ISS analysis on HE materials will be the Kratos 515 CMA high performance analyzer.

E. Ultra High Vacuum Preparation Chamber

A sample preparation chamber with a working pressure range between $10^{-10}$ torr and $\sim$1 atm will be available on the Kratos X-SAM 800 purchased by Mound. This preparation chamber will be directly attached to the hemispherical analyzer (XPS, AES, SAM) chamber by an UHV all metal gate valve. This will allow for samples of HE materials, in particular $TiH_x$, to be prepared in the VHV chamber and analyzed without exposure to the atmosphere. In addition the reactivity of a "freshly" prepared surface, e.g., $TiH_x$, to various gaseous, atmospheric components, such as $O_2$ and $H_2O$, can be examined again in a controlled environment. This preparation chamber will be particularly beneficial in studying rate and stoichiometry of oxidation of $TiH_x$ and the rate of dissolution of the oxide into $TiH_x$. The dissolution studies will be examined as a function of thickness, temperature and time. Thus, the kinetics (rate constants and activation energy) of $TiH_x$ surface oxidation and dissolution will be established. Also programmed temperature studies on surface chemistry changes, from ambient to just-prior-to-ignition, of various $TiH_x/KClO_4$ blends ($0.15 \leq x \leq 1.95$) will

be accomplished in an effort to understand the nature of the Ti-H bond in thermal ignition. Similar studies on thermites and composites will also be attempted with the aid of this UHV preparation chamber which is attached directly to the chamber housing the surface analyzers.

## IV. SUMMARY

Many interesting studies have been performed by Mound on HE materials. HE materials and containers examined and discussed in the text include: (1) the pyrotechnic materials and blends, $TiH_x$, $KClO_4$, Al, $Cu_2O$, $TiH_x/KClO_4$, and $Al/Cu_2O$, (2) the explosives and composites, PETN, RDX and PBX and (3) the iron-nickel alloy HE container. These examinations revealed the great, and possibly unexpected, importance of surface chemistry on accelerated aging and material compatibility. These studies have shown: (1) an understanding of the role surface chemistry plays in pyrotechnic ignition, (2) changes in binder chemistry after coating of the explosive, and (3) the effect $O_2$ plasma and $H_2O_2$ treatments have on the surface stoichiometry and oxide thickness for HE, metal alloy containers. Future studies were outlined in light of the new surface equipment that will be available at Mound.

REFERENCES


1. W. E. Moddeman and W. D. Pardieck, Surface Chemical Analysis, Surface Integrity of Starting Materials, UDRI-TR-75-16, University of Dayton (May 1975).

2. A. Rengan and W. E. Moddeman, ESCA Studies on the Thermite Mixture of Aluminum and Cuprous Oxide Using Mg X-Radiation, UDRI-TR-77-30, University of Dayton (June 1977).

3. A. Rengan and W. E. Moddeman, X-Ray Photoelectron Studies on the Thermite Mixture of Aluminum and Cuprous Oxide. Thickness Measurements of Carbon and of Aluminum Oxide on Aluminum, and Changes in Copper Chemistry, UDRI-TR-78-22, University of Dayton (December 1978).

4. W. E. Moddeman, A. Rengan, P. S. Wang and L. D. Haws, Surface Studies of an Aluminum/Cuprous Oxide Thermite Mixture by X-Ray Photoelectron and Auger Spectroscopies, in Proceedings of 10th Symposium on Explosives and Pyrotechnics, February 14-16, 1979, San Francisco, CA.

5. P. S. Wang, L. D. Haws, W. E. Moddeman and A. Rengan, Aluminum Particle Surface Studies in $Al/Cu_2O$ by Electron Spectroscopy for Chemical Analysis and Electron Spectroscopy, MLM-2664, Monsanto Research Corporation, Mound Facility, Miamisburg, OH (September 1979).

6. P. S. Wang, L. D. Haws and J. A. Peters, X-Ray Induced Auger Electron Spectroscopic Studies on Aluminum Metal Surface Films in $Al/Fe_3O_4$ Thermites, in Proceedings 7th International Pyrotechnic Symposium, Vail, CO, July 14-18 (1980).

7. T. N. Wittberg, W. E. Moddeman, L. W. Collins and P. S. Wang, The Dissolution of Native Oxide Films on Titanium for Pyrotechnic Applications, LeVide, France, 1980, in press.

8. W. E. Moddeman, L. W. Collins, P. S. Wang and T. N. Wittberg, Role of Surface Chemistry in the Ignition of Pyrotechnic Materials, in Proceedings 7th International Pyrotechnic Symposium, Vail, CO, July 14-18 (1980).

9. P. S. Wang, L. D. Haws and W. E. Moddeman, Surface Studies on the Thermite Mixture of Al/$Cu_2O$. III. Scanning Auger Microscopy of the Consolidated Pellet, MLM-2753, Monsanto Research Corporation, Mound Facility, Miamisburg, OH (October 1980).

10. W. E. Moddeman, B. J. Vogt, A. L. Testoni and P. S. Wang, Surface Studies on the Pyrotechnic Oxidizer $KClO_4$, MLM- , Monsanto Research Corporation, Mound Facility, Miamisburg, OH, in preparation.

11. W. E. Moddeman, B. J. Vogt, A. L. Testoni and P. S. Wang, X-Ray Induced Degradation of $KClO_4$, in preparation.

12. W. E. Moddeman, L. D. Haws, T. N. Wittberg and P. S. Wang, Surface Studies on Explosive and Composite Materials, MLM- , Monsanto Research Corporation, Mound Facility, Miamisburg, OH, in preparation.

13. R. G. Copperthwaite and J. Lloyd, J.C.S. Dalton, 11, 1117 (1977).

14. B. L. Henke, J. Phys. C, 4, 115 (1971).

15. T. N. Wittberg, J. R. Hoenigman, W. E. Moddeman and R. F. Salerno, Appl. Surf. Sci., 4, 531 (1980).